Performance of Tyre Cell Foundation as a Sub-ballast Capping Layer under Cyclic Train Loading

Buddhima Indraratna, Ph.D, F.ASCE[1], Fatima Mehmood[2], Trung Ngo, Ph.D, M.ASCE[3], Cholachat Rujikiatkamjorn, Ph.D, M.ASCE[4], Jim Grant[5]

[1]Distinguished Professor of Civil Engineering and Director of Transport Research Centre, University of Technology Sydney, Ultimo, NSW 2007, Australia.
Email: Buddhima.Indraratna@uts.edu.au (Corresponding author)

[2]PhD student, Transport Research Centre, School of Civil and Environmental Engineering, University of Technology Sydney, Ultimo NSW 2007, Australia.
Email: Fatima.Mehmood@student.uts.edu.au

[3]Senior lecturer, Transport Research Centre, School of Civil and Environmental Engineering, University of Technology Sydney, Ultimo, NSW 2007, Australia.
Email: Trung.Ngo@uts.edu.au

[4]Professor, Transport Research Centre, School of Civil and Environmental Engineering, University of Technology Sydney, Ultimo, NSW 2007, Australia.
Email: Cholachat.Rujikiatkamjorn@uts.edu.au

[5]Ecoflex International Pty Ltd, Avoca Beach, NSW 2251, Australia.
Email:jim@ecoflex.com.au

ABSTRACT

This paper presents laboratory and field test results on the use of Tyre Cell Track Foundation (TCTF) consisting of an assembly of infilled rubber tyres to reinforce capping material below the ballast layer. Large-scale cubical triaxial tests were carried out with two different infill materials (crushed basalt rockfill and recycled spent ballast) and they were subjected to varying cyclic loading magnitudes and frequencies. A multi-stage cyclic loading was performed with and without the inclusion of tyre cell reinforcement, whereby the cyclic loading was applied in four different stages with 25,000 loading cycles in each stage. In the first two stages, the frequency was increased from 10 Hz to 15 Hz for an equivalent axle load of 25 tonnes. For the third stage, the axle loading was increased to 35 tonnes with a frequency of 10 Hz, which was then increased to 15 Hz in the final stage. The results showed that the TCTF could reduce the vertical stress transmitted to the subgrade layer as well as curtail the vertical and lateral displacement of the ballast layer. The TCTF further stabilised the track without any significant reduction of the resilient modulus of the overlying ballast as the loading and frequency increased. Compared to a traditional track, the TCTF showed a reduction of 40.1% and 28.3% in the breakage index for the crushed latite basalt and spent ballast (i.e. recycled from ballast tips) infilling the tyre cells, respectively. Test results confirm that the TCTF can significantly improve the overall track performance, and this could be mainly attributed to the increased confining pressure provided by the tyre cell assembly, as well as due to the enhanced damping properties of the rubber tyre inclusions. In addition, the concept of TCTF was tested using a fully instrumented track (20m long) subjected to the passage of a 22-tonne locomotive with two fully loaded carriages. The trial section was constructed within a maintenance yard for heavy-haul rolling stock located in a western suburb of Sydney. Field measurements revealed that, compared to the standard track, the TCTF significantly reduces stress transfer to the subgrade soil. This ultimately mitigates excessive deformation and subgrade failure, making TCTF a sustainable solution for soft and weak subgrade soils despite initial settlement.

Keywords: *Ballast, railway, track deformation, waste rubber tyres, field testing*

Introduction

Railways are a major means of transportation in many countries and as such are widely used for carrying passengers and cargo. The increasing demand for efficient railway systems is driven by the need for faster and more reliable transportation that also reduces operational costs and the environmental impact. One key component of a rail track is the ballast layer which supports the rail-sleeper assembly and helps to control the vertical stress distribution with depth (Selig and Waters 1994, Indraratna et al. 2011, Powrie et al. 2019, Arulrajah et al. 2020, Luo et al. 2023). Excessive degradation and deformation of the track continue to impose substantial maintenance costs. Furthermore, over time ballast suffers from wear (attrition), breakage, and fouling, all of which leads to poor performance and compromised track stability (Powrie et al. 2007, Tutumluer et al. 2013, Wong and Coop 2020).

One of the potential techniques to reduce ballast breakage and enhance track stability is the use of artificial inclusions in the track substructure. Utilizing waste rubber tyres in track substructures presents an environmentally friendly approach, mitigating landfill disposal (Presti 2013), while repurposing them for a technologically advanced method of track construction (Maciej 2017, Indraratna et al. 2024). It is estimated that more than 1.4 billion tyres are sold each year leading to a significant increase in the amount of waste rubber (Sienkiewicz et al. 2012). In Australia alone, 50 million equivalent passenger units (EPU) of tyres entered the waste stream in 2009-2010 period (Brindley et al. 2012). The improper disposal of waste tyres has serious consequences, including the potential spread of diseases such as dengue and malaria when tyre stockpiles accumulate rainwater, and considerable air pollution caused by tyre incineration (Mountjoy 2012, Riyajan et al. 2012).

The use of waste rubber in railway tracks has already been examined in a variety of forms including: (i) Rubber crumbs - small particles of crushed rubber mixed with traditional ballast material (Sol-Sánchez et al. 2015, Guo et al. 2019, Arachchige et al. 2022, Wang et al. 2022, Qi and Indraratna 2023, Guo et al. 2019, Koohmishi et al. 2021), (ii) Under ballast mats - large mats made from waste rubber that are placed beneath the ballast layer to provide additional support and cushioning for the rails (Navaratnarajah et al. 2018, Qiang et al. 2023, Ngo et al. 2024, Sheng et al. 2020, Zhao and Ping 2018), among others, (iii) Under sleeper pads - small pads made from waste rubber that are placed beneath the sleepers to improve their stability and reduce vibration (Le Pen et al. 2018, Jayasuriya et al. 2019, Esmaeili et al. 2020, Ngamkhanong and Kaewunruen 2020, Moubeké et al. 2021), and (iv) Neo ballast – a substitute for traditional ballast aggregates made entirely from recycled rubber particles (Fontserè et al. 2016, Sol-Sánchez et al. 2018, Jing et al. 2019). The performance of these recycled rubber components was evaluated under various loading conditions in laboratory settings, confirming their suitability for railway applications (Signes et al., 2017; Qi et al., 2024, among others). Additionally, field tests were conducted to validate the feasibility and practicality of this innovative and sustainable approach (Indraratna et al., 2024; Sol-Sánchez et al., 2015; Luo et al., 2023). This eco-friendly solution not only reduces waste but also enhances the efficiency and durability of rail infrastructure, representing a significant advancement towards a greener and more resilient transportation network (Indraratna et al., 2022; Cai et al., 2020).

Above studies have indicated that the use of recycled rubber can increase the overall performance of railway tracks effectively. A recent technique that was invented by the authors is the use of a Tyre Cell Track Foundation (TCTF); this involves removing one of the side walls of a waste rubber tyre to create a hollow structure that is then filled with granular materials and compacted. In recent years, these infilled tyre cells have been placed in track in lieu of a traditional capping layer to provide greater confinement to the track substructure, while exploiting the increased damping properties or the cushioning effect of rubber (Indraratna et al. 2017, Indraratna et al. 2018, Indraratna et al. 2022). While the TCTF does not require heavy mechanical processing like other applications of waste rubber, their use in rail tracks will require geotechnical engineering analysis of the existing and proposed parameters to ensure the design and construction is fit for purpose. The TCTF is still a relatively new technology that requires further research to quantify its performance when subjected to multistage loading.

Introduced initially by Indraratna et al. (2017), plate loading tests have shown that TCTF could (i) improve the load bearing capacity of the track, (ii) increase the stiffness of sub-ballast by about 50%, and (iii) reduce the stress transferred to the subgrade. Using large-scale testing, Indraratna et al. (2018) further assessed the effectiveness of TCTF under cyclic loading (40-tonne axle load at a frequency of 15 Hz for 500,000 loading cycles) with two types of infill materials. These findings indicate that TCTF actively limits the lateral spreading of ballast particles and reduces the permanent settlement. TCTF improves the damping properties of the system, which in turns can reduce the degradation of ballast, thus enhancing track longevity.

In the previous study (Indraratna et al. 2018), TCTF could only be tested with a ballast thickness of 150 mm due to the size limitation of the prismoidal testing chamber, where 1:1 scale track section could be tested to simulate the stress-strain behaviour closer to reality. Apart from this, only 1 combination of loading frequency and axle load was tested, thereby the broader effects of loading and frequency on the performance of tyre cell were not captured. Nevertheless, it is important to note that the current study focuses on the performance of TCTF with two different infill materials subjected to multistage loading and frequency conditions, utilising a modified prismoidal track process simulation apparatus (1000 mm in depth; 800 mm in the transverse direction; 600 mm in the longitudinal direction), with an overlying ballast layer of 300mm in thickness and a subgrade thickness of 350 mm. In addition, this study includes field testing to demonstrate an original conceptual design of Tyre Cell Track Foundation (TCTF) subjected to actual train loading. The field data captures the role of subgrade soil depth, whereas the laboratory cubical chamber is restrained by a non-displacement (rigid) boundary located about 1m below the surface, thus leading to a constrained vertical stress propagation compared to most field conditions.

Laboratory Testing Program

Large-scale track process simulation apparatus

In this study, a large-scale track process simulation apparatus designed in-house was used to simulate the cyclic loading conditions in track. The dimensions of the test box are 1000 mm in height, with a plan area of 800 mm x 600 mm. Exploiting double symmetry, this represents a unit cell of a track [Fig. 1(a)]. The dimension of 800 mm in the transverse direction represents 1/3 of the Australian standard gauge with a sleeper length of 2400 mm, while the longitudinal dimension of 600 mm represents the typical sleeper spacing (Indraratna et al. 2015). Compared to conventional triaxial testing equipment that applies fluid pressure to control the confining stress, this equipment allowed two walls perpendicular to a sleeper length to be moveable upon applied loading while a specific lateral pressure can be maintained to simulated track's in-situ stress conditions. The height of 1000 mm is sufficient to allow the placement of all track substructure layers including a standard ballast thickness of 300 mm [Fig. 1(b)]. This test apparatus also includes a control unit that operates the loading mechanism (dynamic actuator) which applies the pre-desired cyclic loading to simulate the passage of a train at constant speed. The cyclic load applied by the servo-hydraulic actuator [Fig. 1(a) and Fig. 1(f)] through a 100 mm diameter cylindrical steel ram was transmitted to the ballast layer by a rail-sleeper assembly [Fig. 1(b)]. This test assembly is also equipped with various instrumentation devices (e.g. settlement pegs, lateral displacement transducers, strain gauges, and pressure plates), connected to a fully automated, multi-channel data acquisition system. A thin layer of Teflon spray (anti friction dry PTFE lubricant) was applied on the four side walls of the testing chamber before materials' placement. Based on the calibration using a pressure plate in relation to applied vertical load, the pressure loss at the bottom of the ballast layer was expected to be negligible.

Materials Tested

The test materials used in this study included fresh ballast, TCTF (infill and tyre cell), subgrade soil, and geotextile. The fresh ballast (latite basalt) collected from a quarry south of Sydney consisted of coarse angular aggregates. The ballast was washed, sieved, and prepared according to the Australian standard gradation following AS 2758.7 (2015). Two different materials were used as infill for the tyre cell, namely: (i) Capping-1 consisted of crushed basalt aggregates mimicking sandy gravel, well-graded with a maximum nominal size of 20 mm, as required by Transport for NSW, and (ii) Capping-2 was made of recycled ballast aggregates collected from a railway waste stockpile. Although the gradation of Capping-2 was similar to that of ballast, it did not meet the angularity specifications and was therefore used as sub-ballast. A hydrometer test has been conducted on the subgrade materials, followed the ASTM D7928 (2017) to determine particle size distribution, and the subgrade was mostly categorised as silty sands representative of the coastal terrains. The particle size distribution curves of these materials are shown in Fig. 2, and their physical properties including d_{max} (maximum particle size), d_{min} (minimum particle size), d_{50} (mean particle size), C_u (coefficient of uniformity), C_c (coefficient of curvature), and γ_b (bulk density) are given in Table 1.

Preparation of infilled tyre cells

Tyre cells were cut from used passenger car tyres with an external diameter of 560 mm, a rim diameter of 330 mm, a width of 165 mm, and the tyre cell thickness of 10 mm. The tread width of 165 mm conveniently served as the vertical dimension of the infilled tyre cell replacing the traditional capping layer that is usually 150mm in thickness in Australian heavy haul tracks. A layer of geotextile was also used at ballast-capping and capping-subgrade interfaces as a separator to prevent different materials from mixing, for instance the upward migration of subgrade soil particles under cyclic loading. One side wall of the tyre (top) was removed to facilitate convenient filling and compaction of the infill material, whereas the other side wall (bottom) remained intact to maintain stability of the cell with sufficient base friction. To determine the stress-strain relationship of the tyre as per ASTM D4885 (2018), four samples were extracted from the tread of the tyre and then cut into an I-shape. The samples from a tyre tread represent the actual composite rubber and radial steel similar to those used in the experiment and field test. When sections of the tread are cut along the thread, they resemble an 'I' shape to clamp the wider flange in the test clamps. The flanges were then fixed inside the test machine clamps such that the web part had a width of 40 mm and the gauge length was kept at 80 mm. These samples were tested under uniaxial tension at a strain rate of 2.5%/min. Results of these uniaxial tensile tests are shown in Fig. 3(a) where the average tensile stress at 2% strain was 6.4 MPa, whereas that at 5% strain was 15.9 MPa. Fig. 3(b) shows the dynamic mechanical analyser (DMA) used to determine the damping ratio of the rubber samples having a thickness of 5mm and a diameter of 10-12 mm [Fig. 3(c)]. Test results showed that the damping ratio for the rubber samples was in the proximity of 0.21. It is noted that tyres are not easily ignitable and require oxygen to burn, neither of which are present when they are buried under 250 mm of railway ballast. Goryunov et al. (2019) demonstrated that tyres meeting proper Australian standards can withstand operational temperatures of up to 100°C (max. 120°C), while their combustion point is above 350°C. In general, the thickness of the capping layer in Australian heavy haul tracks is in the range of 150-200 mm. To ensure a fair comparison, tyres with similar widths were chosen, and the selected car tyres had a width of

@ 200mm. Depending on the thickness of this layer, various types of tyres, including passenger car tyres, 4WD tyres, light truck tyres, and truck tyres, can all be engineered into these tyre cell structures.

Test program and sample preparation

The test specimens were prepared as per the track profile shown in Fig. 1(b), with and without the inclusion of the tyre cell. Multistage cyclic loading was conducted in four different stages for each test, as detailed in Table 2. Different stages of specimen preparation are illustrated in Fig. 4. Firstly, the subgrade material was filled inside the test box and compacted in three sub-layers to a unit weight of 17.5 kN/m^3 and a total thickness of 350 mm, using a hand-held vibratory compactor. A pressure plate was placed on the top of compacted subgrade to measure the vertical stress, followed by a layer of geotextile [Fig. 4(a)]. This was then followed by placing a 200mm thick compacted capping layer. A tyre cell [Fig. 4(b)] (with biaxial strain gauges attached) was placed above the layer of geotextile for the reinforced samples. For the unreinforced sample, Capping-1 material was compacted to a unit weight of 21.6 kN/m^3. The tyre cell was infilled with the pre-made granular materials as shown in Fig. 4(c and d) (i.e. Capping-1 for Test 2 and Capping-2 for Test 3) which were compacted to the desired unit weight as mentioned in Table 1. Upon applying cyclic loading, the tyre cell filled with infill material would undergo vertical compression and outward radial expansion, exhibiting two degrees of freedom. This outward radial expansion induces hoop stress, which subsequently provides additional confinement to the infill within the tyre cell. After preparing the capping layer, a pressure plate was placed followed by a geotextile as a separator. A 300 mm thick ballast was then placed on top of the geotextile layer simulating the actual track conditions. The ballast layer had been prepared to the Standard grading limits and compacted to a unit weight of 15.6 kN/m^3 [Fig. 4(e)]. A concrete sleeper-steel rail assembly was then placed on the ballast surface, and finally crib ballast placed and lightly tamped to be in level with the sleeper surface.

The test chamber was then positioned in the loading frame with an axial dynamic actuator. A lateral confining pressure of 15 kPa was applied to the specimen in the transverse lateral direction (i.e., parallel to the sleeper), emulating typical in-situ confinement of 10-20 kPa measured in most Australian ballast tracks (Indraratna et al. 2011). Displacement in the longitudinal direction (i.e. perpendicular to the sleeper) along the track was restrained, simulating a plane strain condition with no lateral displacement. The axial cyclic load was applied incrementally to avoid any damage to the actuators. The track settlements, lateral displacement and vertical stresses were continually recorded during the testing phase.

Applied cyclic loading program

The performance of track specimens was investigated using four different cyclic loading stages. To calculate the cyclic stress ($\sigma_{1_{cyc}}$), Equation 1 (AREA 1974, Jeffs and Tew 1991) and Equation 2 (Raymond 1977) were used as follows:

$$\sigma_{1_{cyc}} = \left(\frac{2q_r}{Bl}\right) F_2 \qquad (1)$$

$$q_r = 0.5P \qquad (2)$$

where q_r = rail seat load, P = design wheel load = ½ Axle load, B = sleeper width, l = sleeper length, F_2 = Typical values of F_2 between 2 and 3 have been recommended by various rail organisations; a value of $F_2 = 3$ was used for the load calculations. Jeffs and Tew (1991) showed that the uniform contact pressure between the sleeper and ballast is generally assumed within the effective sleeper length which is 1/3 of its total length. In this study, the sleeper length is

0.68m and width is 0.22 m to fit inside the testing chamber. The maximum magnitude of load applied from the vertical actuator can be calculated to be F_{max}=35.2 kN and F_{max} = 49.3 kN for 25 tonne and 35t tonne axle load, respectively.

The cyclic load was applied on the top of the steel rail through a steel load cell attached to the vertical dynamic actuator [Fig. 4(f)]. The details of cyclic loading scheme are shown in Fig. 5. In the first and second loading stages, the maximum loading magnitude was kept at $\sigma_{1cyc,max}$ = 235 kPa, which corresponds to a 25-tonne axle load. The loading frequency was increased from f=10 Hz to 15 Hz to assess the role of increasing train speed. Considering a standard gauge Australian track and typical axle arrangement of a freight train, this will represent the increase in speed from about 70 km/h to 110 km/h (Indraratna et al. 2015, Indraratna et al. 2018). In the third and fourth stages, the loading magnitude was increased to $\sigma_{1cyc,max}$ =330 kPa, which corresponds to a 35-tonne axle load, while the loading frequency was increased from f=10 Hz (Stage 3) to 15 Hz (Stage 4). There was a short rest period (0.5 hour) between the different loading stages for taking data measurements and adjusting the applied loading and frequency. The increase in vertical deviator stress was necessary to investigate the influence of axle load on ballast behaviour including deformation and particle breakage.

Results and discussion

Measured settlement and lateral displacement

Figure 6a shows the total track settlements measured at different loading cycles (N) for all three tests. As expected, when loading commenced, all the tests exhibited a sudden increase in settlement up to N=1000 cycles due to particle re-arrangement. In stage 1, Test 1 (without a tyre cell) shows greater deformation than Tests 2 & 3 with the TCTF. However, in Test 2

(Capping-1 infilled with a tyre cell), the rate of deformation stabilizes after *N*=1000 cycles while that of Test 3 (Capping-2 infilled with a tyre cell) tends to increase continually, but at a slower rate. At the end of Stage 1 (*N*=25000 cycles), the overall settlement of the track model with TCTF is smaller than that of the unreinforced test (i.e. without a tyre cell). As the test progresses towards Stage 2 (loading frequency increased to 15 Hz), there is a slight increase in track settlement until *N*=26000 cycles; followed by swift stabilisation for all three tests. In comparison, the specimen with TCTF shows less track settlement (9.4 mm for Capping-1 and 10.5 mm for Capping-2) compared to the unreinforced track at the end of Stage 2 (11.2 mm). The results from Stages 1 and 2 indicate that the increased loading frequency results in an increase in track settlement. This observation also indicates that at a lower loading range (up to 25 tonnes), TCTF helps to reduce track settlement with both types of infill materials.

At the start of Stage 3 (loading increases from 25 to 35 tonnes), all specimens experience a pronounced increase in settlement up to *N*=60,000, beyond which the rate of settlement decreases. However, Test 3 (TCTF with Capping 2) experiences the highest settlement, probably attributed to the increased stresses at the contact points of the spent (recycled) ballast causing the particles to break, displace, and undergo particle re-arrangement of the granular mass. It could also be partly due to a reduction in the apparent friction angle and the particle interlocking of spent ballast (Bolton et al. 2008). In Stage 4, the increase in loading frequency causes all specimens to experience a slight increase in settlement, where the unreinforced specimen shows the highest settlement. The total settlements of the unreinforced test (Test 1) and tyre-cell reinforced capping-2 (Test 3) are almost the same at the end of the test (18.6 mm and 18.5 mm, respectively). The specimen with tyre-cell reinforced Capping-1 (Test 2) is the most stable, showing insignificant increase in deformation during the final loading stage; reaching a total settlement of about 15.1 mm that is lower than that of all the other tests. Results from Stages 3 and 4 also demonstrate the pronounced effect that the loading magnitude has on track settlement compared to the frequency.

Figure 6(b) shows the measured lateral displacement (in transverse direction) of all tests. The results indicate that an increase in the loading magnitude and frequency affects the lateral displacement similarly to track settlement. For instance, in Stages 1 and 2, the specimen with capping-2 experiences the lowest lateral deformation of around 0.55 mm, while the specimen with capping-1 exhibits a lateral displacement of about 0.84 mm. The tyre+capping-2 (spent ballast) performed better than the tyre+capping-1 (crushed basalt) in these loading stages, which can be attributed to the combined effect of internal interlocking of large aggregates (spent ballast) and the additional confinement provided by the tyre cell that arrests lateral movement.. In Stage 3, with an increase in the loading magnitude, Test 1 (without tyre cell) shows the highest lateral movement of about 3.08 mm, while Tests 2 &3 (with Capping-1 and Capping-2) exhibit lateral displacements of approximately 2.59 mm and 2.23 mm, respectively. The accumulated lateral displacements at Stage 4 of the reinforced specimens (Test 2, 3) are less than that of the unreinforced case (Test 1) which shows an increasing trend of lateral strain accumulation. Not surprisingly, the test data also prove that less deformation is observed for the specimens with the tyre cell that offers additional confinement as further elaborated below.

The use of Capping-2 material (spent ballast) has been carried out previously by the first author in the laboratory (Indraratna and Salim 2003, Indraratna et al. 2018) as well as in field testing (Indraratna et al. 2010). Test results have demonstrated that the recycled ballast has a lower tensile strength compared to fresh ballast and, hence requires geosynthetic reinforcement if used in practice. The reduced strength of the aggregates makes recycled ballast more vulnerable to breakage upon loading. Recycled ballast exhibits > 95% higher breakage compared to fresh aggregates, and therefore it cannot be considered as the main load-bearing layer. However, with the inclusion of a reinforcement layer (e.g. woven geotextile, geogrid), the settlement of recycled ballast decreases to an acceptable level. Field testing on recycled ballast (Indraratna et al. 2010) further proved that when reinforced with a geocomposite, the corresponding track shows less settlement compared to a standard ballast track. Recently, spent ballast (Capping-2) was tested in the laboratory as a control test by Indraratna et al. (2018). The test results showed that there was an increase in settlement by about 10 mm when spent ballast was used in contrast to conventional capping material (crushed basalt). At N=100,000 cycles, Capping-2 exhibited a lateral displacement of about 7.2 mm while the crushed basalt capping showed insignificant lateral displacement [(Fig. 6(b)]. However, when capping 2 material (recycled ballast) was confined within the tyre cells, a substantial reduction in lateral displacement was observed to be in par with Capping 1 material. More details about test results can be found in Indraratna et al. (2018). According to track design guidelines specified by Transport for NSW and previous tests conducted on recycled ballast (i.e., discarded after track maintenance), the spent ballast that is usually substantially degraded (i.e. reduced size, less angularity and less interlocking friction when compacted), is recommended on its own as a capping material.

Additional confining pressure and mobilised strain in tyre cell

Upon loading, the tyre cell expands and generates hoop stress that provides additional confining pressure to the infilled material, resulting in enhanced stability and load-bearing capacity of the substructure. This additional confining pressure also helps the track to resist lateral deformation and settlement over time (Lackenby et al. 2007). In order to determine the additional confining pressure provided by the rubber tyre cell, the cell wall was equipped with biaxial strain gauges, which enabled the measurement of axial and circumferential (hoop) strains, as shown earlier in [Fig. 4(b)]. The variations in circumferential strain in the tyre cell wall with the number of cycles for both capping infill materials (Tests 2 & 3) are shown in Fig.

7(a)]. Measured circumferential and axial strains indicate tension in the lateral direction and compression in the vertical direction, respectively.

In Stage 1, the mobilised circumferential strain is approximately 0.25% caused by the placing and compaction of the infill plus the effect of overburden stress applied by ballast; this then increased to 0.35% as the load was applied. In Stage 2 (frequency increased to 15 Hz), the strain increases slightly to 0.39%. When the loading magnitude increases in Stage 3, the tyre cell reaches a maximum circumferential strain of about 0.43% and remains almost unchanged until the end of testing. The axial compressive strains in the tyre cell are relatively small in the vicinity of 0.01%, and this can probably be attributed to the significant rigidity of the rubber tyre cell in compression.

The measured circumferential strains can be used to calculate the additional confining pressure ($\Delta\sigma_3$) , using the hoop tension theory introduced by Henkel and Gilbert (1952).

$$\Delta\sigma_3 = \frac{2M\varepsilon_c}{D_\varepsilon}\left(\frac{1}{1-\varepsilon}\right) \quad (3)$$

where, $\Delta\sigma_3$ = additional confining pressure, M = extension modulus of the tyre cell (M =1335 kN/m as measured in the uniaxial tension test), ε_c = mobilised circumferential strain of the tyre, D_ε=diameter of tyre cell at the strain ε_c, ε = axial strain in the infill materials.

Fig. 7(b) shows the calculated additional confining pressure ($\Delta\sigma_3$) provided by the tyre. During the first two initial stages, the $\Delta\sigma_3$ increases from 12.5 kPa to 18 kPa. With an increase in the cyclic loading in Stages 3 and 4, $\Delta\sigma_3$ increases to 20.5 kPa. Indraratna et al. (2017) found that an increase in confining pressure generated by a rubber tyre cell could improve the durability and performance of a capping layer. The lateral confining pressure (minor stress) at the perimeter of the unit cell (i.e. beyond the tyre cell) was applied in the transverse direction (parallel to sleeper) by external hydraulic jacks, and this stress was kept unchanged as σ_3=15 kPa during the test. The axial strain in the infill materials within tyre cell was measured by settlement pegs that were installed at the top surface and bottom level of the infill-capping material. In this apparatus the side walls are not rigid as they can move on frictionless casters and the lateral displacements and lateral pressures change according to the applied cyclic loading mimicking real-life conditions (Indraratna et al. 2011). Therefore, unlike testing conducted within a rigid box, the stress-strain behaviour of the materials confined in this prismoidal testing chamber is more realistic. The sides of the box are free to displace upon the application of the external cyclic stresses, where the vertical stress represents the train axle load, and the frequency of load is a function of the train speed. Therefore, the internal deformation of the infilled granular medium within the flexible tyre cell will influence the corresponding internal stresses accordingly. In other words, a tangential hoop stress develops around the rubber tyre cell (measured by bonded strain gauges to the interior of the cell wall) and the corresponding radial stresses develop within the infilled material as the rock aggregates deform during the application of this repeated (cyclic) loading.

It is noteworthy that dilation of the infilled material can still occur as the transverse direction (parallel to the sleeper) moves significantly more than the longitudinal direction (perpendicular to the sleeper), hence approximating a quasi-plane strain condition like in a real-life track, where the strain in the longitudinal direction (i.e. direction of train passage) is relatively small due to the confinement provided by the concrete sleepers. If the cumulative lateral strains exceed the vertical strain, then the internal material becomes dilative, and if the vertical strain is greater than the cumulative lateral strains, then the material becomes contractive. Measured results have shown that greater the dilation of the aggregates infilling the tyre cell, greater the hoop stress and the vice versa. It is of course possible for the stresses and strains of fill materials inside the chamber to vary in relation to the boundary displacements (and stresses), unlike in a rigid box where zero movement of the boundaries of the box will not generally effect stress changes of the material within the box.

Resilient Modulus

The resilient modulus (M_R) of ballast is an important parameter that is commonly used to characterize the load-deformation response of ballast under cyclic loading. Fig. 8 shows how the resilient modulus M_R, can be determined by utilising the loading-unloading curves. During each loading stage, bursts of data were recorded at specific loading cycles to determine the resilient modulus (M_R) as follows:

$$M_R = \frac{\Delta q}{\varepsilon_{a,rec}} \qquad (4)$$

where, the deviator stress (Δq) is determined as the difference between the maximum and minimum cyclic stress [Fig. 8(a)], and the recoverable axial strain ($\varepsilon_{a,rec}$) that is determined based on the deformations measured on top of the ballast layer (by subtracting the axial strains of the loading-unloading cycle), as shown in Fig. 8(b).

Fig. 9 shows the variations of resilient modulus (M_R) with the number of loading cycles during 4 loading stages. In Stage 1, ballast aggregates experience an initial compaction with a rapid increase in M_R to around 280 MPa within 1000 cycles [Fig. 9(a)]. The rate of increase then decreases as the number of cycles approaches N=25,000. The M_R of ballast for the unreinforced specimen (Test 1, M_R=339 MPa) is higher than that of the reinforced specimens (e.g., M_R=302 and 316 MPa for Tests 2 & 3, respectively). However, as the loading frequency increases to 15 Hz in Stage 2, a slight drop in initial M_R is observed [Fig. 9(b)], and this is because higher loading frequencies lead to a greater extent of vibration, which in turn can increase ballast deformation (Sun et al. 2019). However, as the number of cycles increases, the value of M_R

also increases and begins to stabilise towards the end of Stage 2. The value of M_R of the unreinforced sample (Test 1) remains higher than that of the reinforced specimens, but it is noteworthy that the difference is not as significant when compared to Stage 1.

In Stage 3, as the loading magnitude increases to 35 tonnes, the value of M_R decreases significantly for all tests, as the ballast aggregates experience further deformation under increased load [Fig. 9(c)]. However, these values increase rapidly after 1000 cycles (i.e. N=51,000), followed by a gradual increase towards the end of the loading stage. The magnitudes of M_R of the reinforced specimens (i.e. M_R=275 and 278 MPa for Tests 2 and 3, respectively) are higher than that of the unreinforced specimen (M_R=258 MPa); these observations verify the effect of TCTF at higher loading. In stage 4, for the reinforced specimens there is only a slight reduction of 3.7 % in M_R but it regains its magnitude as the number of loading cycles increases to N = 80,000 cycles [Fig. 9(d)]. With the unreinforced specimen, the drop in resilient modulus is noticeable to about 214 MPa, but yet it increases with the number of loading cycles after N=75,000 cycles.

It is observed that in the first two stages, the resilient modulus is higher for the unreinforced condition, whereas in the last two stages, the opposite is observed. This is probably attributed to insufficient compaction of the infill materials inside the tyre cell, causing higher elastic strains initially until the infill aggregates become denser with time with increasing number of loading cycles. It is found that excessive tamping of particles inside the tyre cells would lead to increased breakage and therefore the compacted unit weight of the aggregates within the tyre cells was kept to about 16 kN/m^3 to minimise particle breakage during tamping. Practically, with the inclusion of tyre cells, initial track settlement may be high as the infill materials continue to undergo significant compression. Track settlement is stabilised once the confinement provided by tyre cells is fully mobilised, providing maximum lateral confinement and enhanced stiffness. Overall, TCTF can provide a more stable foundation where there is no substantial decrease in the resilient modulus of ballast with increased magnitudes of loading and frequency.

Damping Ratio and Dissipated Energy

Ballast aggregates subjected to cyclic loading display a distinct hysteresis response where mechanical strain energy is stored and then dissipated during the loading-unloading process. Including the TCTF can certainly improve the damping characteristics of the system under dynamic loads (Indraratna et al. 2018). Energy reservoirs offered by the rubber can reduce the amplitude of the vibrations and noise generated by the train, thus improving the ride comfort and reducing the rate of deterioration of track components. Hysteresis loops are plotted at a selected number of loading cycles (*N*) for 3 tests as shown in Fig. 10(a)-10(c). It is seen that the inclusion of a tyre cell increases the subtended area of the hysteretic loops. For instance, at N=50 cycles, the area subtended by the hysteresis loop was highest in Test 2, followed by Test 3, and then the unreinforced sample (Test 1). This shows that including the tyre cells can improve energy dissipation through enhanced damping properties of the track substructure.

The energy dissipation and damping ratio can be determined as shown schematically in Fig. 10(d), based on ASTM D3999 (2003). In relation to the hysteresis loops, the dissipated energy (E_d) for each test was calculated and presented in Fig. 11. In Stage 1, within 1000 cycles, E_d decreases with the number of cycles due to the high dissipation of energy because of the re-arrangement and associated compaction of ballast. Test 1 (without a tyre cell) shows the value of E_d to be about 48 J/m^3, which is slightly lower than those specimens having a tyre cell (i.e. Test 2: 55 J/m^3; Test 3: 52 J/m^3). In Stage 2, the increase in loading frequency causes the E_d to decrease slightly in the initial cycles, and then almost stabilize towards the end of the loading stage. The value of E_d remains higher for the reinforced specimens than that of the unreinforced counterpart, but the difference is not as significant as in the subsequent loading stages. In Stage 3, with an increase in the loading magnitude, the dissipated energy increases rapidly in the first 50 cycles. However, as the number of loading cycles increases, this energy level decreases and tends to stabilise at about 97 J/m^3 (Test 2) and 85 J/m^3 (Test 1). The increased frequency in Stage 4 has a slight effect on the reinforced specimens but causes a significant decrease to about 68 J/m^3 for the unreinforced Test 1.

The variations of damping ratio (*D*) of three tests measured at different loading stages are shown in Fig.12. In Stage 1, both reinforced and unreinforced tests show an average damping ratio of 0.20 and 0.18, respectively. With the increase in frequency (Stage 2), the damping ratio in all tests decreases slightly to 0.18 (Test 2) and 0.16 (Test 1). There is no significant change in damping ratio in subsequent loading Stages 3 &4 for which the damping ratio is about 0.15 for the tests with tyre cell. In contrast, there is noticeable drop in damping ratio for the unreinforced specimens to about 0.10. In a practical perspective, these results imply that placing a rubber tyre cell assembly in heavy haul tracks can offer increased damping of the substructure leading to a reduction in ballast breakage.

Measured stress distribution with depth

Pressure plates were placed at the interface of the sleeper/ballast, ballast/capping and capping/subgrade to measure the vertical stress propagation along the depth. The vertical stresses for all three tests at *N*=100,000 (corresponding to a 35-tonne load) are shown in Fig. 13. These measurements show that while the vertical stresses decrease with depth, the stresses at the sleeper-ballast interface of the unreinforced specimen (Test 1: σ_v = 311 kPa) was higher than those of the reinforced specimens (σ_v = 256 kPa and σ_v = 287 kPa for Test 2 (Capping 1) and Test 3 (Capping 2), respectively). The overall values of stiffness of the tested samples were different (i.e., different caping materials, and with/without the presence of the tyre cell), resulting in a corresponding variation of the measured stresses at the sleeper-ballast interface. As explained above, this is an application of dynamic loads with moving external boundaries, hence this process replicates real-life track conditions where the internal stresses of the infilled material do change when the sides of the chamber displace under the applied cyclic loading. A controlled loading mechanism was employed through dynamic actuator that adjusts the applied force using feedback systems in real-time. The internal stress changes were measured by the pressure cells placed inside the testing chamber (box) in both vertical and horizontal positions, as well as strain gauges bonded to the tyre cell wall. These results have been plotted to explain the behaviour in Figures 7 & 10, and discussed in detail previously. The TCTF enhances the stiffness of capping, hence increasing the stresses measured at the top of capping layer (σ_v = 126 and 146 kPa for Test 2 (Capping 1) and Test 3 (Capping 2), respectively, as compared to σ_v = 122 kPa for Test 1). The vertical stress had transmitted to the top of subgrade for Test 1 was 67 kPa (without tyre cell), but only 44.5 kPa and 49.7 kPa for the reinforced specimens in Tests 2 and 3, respectively. This indicates that the TCTF enables a stress reduction of about 34% and 26% measured at the top of subgrade, and the increased damping of TCTF also helps to reduce the stress transferred to the underlying layers.

It is noted that due to the lack of sufficient planar space that can restrict the development of an accurate pressure bulb in the controlled laboratory tests. However, in this apparatus the side walls are not rigid as they can move on casters and the lateral displacements and lateral pressures can be measured (Indraratna et al. 2011). In the field, the stress disperses and transfers naturally to underneath substructure layers, resulting in potentially different stress patterns compared to what can be simulated in the lab. There are always differences in both boundary effects and scale effects, which make the laboratory different to field data. Given that the geotechnical community is fully aware of the scale-effect limitations in experimental geomechanics, field trialling is the best solution to alleviate the potential limitations of laboratory testing in relation to both boundary effects and scale effects. A more comprehensive and reliable set of results could be obtained through a fully instrumented field trial in contrast to the laboratory environment.

For comparison, the stresses measured in the field and lab tests are also included in Fig. 13. The field tests performed at the Bulli track (Indraratna et al. 2010) and a study carried out by Rose et al. (2004) correspond to 25 and 40-tonne axle loads, respectively. In this laboratory test, the stresses measured under the sleeper (278 kPa) are in reasonable agreement with those obtained from the field (Indraratna et al. 2010, Rose et al. 2004). In contrast, stresses at the top of the capping layer (110 kPa) obtained from this study have notable variations with the field tests, and this may be attributed to inevitable differences in capping layer stiffness and boundary conditions. It is noteworthy that the above-mentioned stresses are also in reasonable agreement with the laboratory tests performed by Qi and Indraratna (2023) for axle loading of 25 tonnes.

Ballast Breakage

The ballast breakage index (BBI) introduced by Indraratna et al. (2011) was used to measure the degree of degradation or fragmentation of ballast aggregates. The BBI can be calculated by comparing the particle size distribution of ballast before and after testing, as shown in Fig. 14 and Table 3. After visually examining and then sieving the tested ballast, it is seen that the most noticeable modes of breakage include particle splitting, corner breakage, and attrition of the edges, and the greatest damage is in the 37.5mm size range. The inclusion of TCTF with capping-1 (crushed basalt) and capping-2 (spent ballast) leads to a reduction in BBI of 40.1%

and 28.3%, respectively. In a practical point of view, these results indicate that rubber tyre cells improve the stability of tracks by increasing the confinement of the infilled granular materials while providing enhanced damping of the track, both of which lead to a reduction in ballast breakage.

In this study, the track process simulation testing carried out on a single infilled tyre representing the unit cell concept (Indraratna et al. 2017) demonstrated a significantly improved performance of the track element under cyclic loading. However, these test results alone cannot be applied to accurately predict the field behaviour that benefits from a multi-tyre assembly with distinctly different real-life moving loads and boundary effects (e.g. the depth of subgrade in the field). So, while the single tyre testing was useful in demonstrating the concept, a more comprehensive and reliable set of results could be obtained through a fully-instrumented field trial in contrast to the laboratory environment. The field data capture the role of subgrade soil depth, whereas the laboratory cubical chamber is restrained by a non-displacement boundary located about 1m below the surface, thus leading to a constrained vertical stress propagation compared to reality.

Field Application of TCTF

An instrumented track (20m long) was constructed within a maintenance yard for heavy-haul rolling stock in Chullora, a suburb of Western Sydney [Fig. 15(a)], in collaboration with Transport for NSW (State Government) and Ecoflex International. For the first time in the world, this field trial promoted the concept of Tyre Cell Track Foundation (TCTF) in lieu of a traditional capping layer (compacted well-graded sandy gravel). In each tyre cell, the top sidewall was removed for ease of compaction when filled with recycled spent ballast that was equivalent to Capping-2 material used in the laboratory. A cross-section of the TCTF is schematically illustrated in Fig.15(b). The performance of the TCTF track could be compared with an adjoining standard track also 20 m long. The TCTF section was strategically located in an area where the heavy haul trains decelerate quickly when approaching the maintenance yard, so this is a section where track movements and stresses need to be controlled effectively.

Site Geology, Track Construction and Loading

Field reconnaissance included the drilling five boreholes (BH 1 to BH 5) in accordance with the Australian Standard, AS 1726 (2017) for geotechnical site investigations. The subsurface strata comprised a compacted granular fill (500 mm in thickness) that was placed above the natural subgrade consisting of a thin layer of sandy clayey silt of low plasticity (PI = 12%), followed by residual silty clays and claystone gravel overlying a stiff clay deposit, and then the bedrock of mainly weathered shale (approx. 3.8m m below the base of the TCTF). Although the water table in this area was generally about 5 m below the ground surface, the subgrade beneath the TCTF was found to be saturated due to medium to heavy regular rainfall and impeded subsurface drainage. The soft and saturated subgrade soil in this area was known to be vulnerable for excessive undrained yielding and mud pumping (Sydney Train Report 2021), hence the role of TCTF was expected to carry a significant vertical stress and thereby attenuate the load propagation to the deeper soft subgrade.

Off-the-road truck tyres were delivered to the testing test site and placed in a honeycomb pattern over the compacted fill and then infilled with discarded ballast recycled from a stockpile. These infilled rock aggregates were compacted using a vibratory roller passing over the TCTF section to a unit weight in the proximity of 16.0 kN/m^3. The adjoining standard section had a conventional granular capping layer consisting of a compacted sandy gravel up to 200mm in thickness (unit weight approaching 17 kN/m^3), and levelled with the top surface of the TCTF.

A feasibility study from an environmental perspective on the effect of the TCTF on groundwater contamination is out of the scope of this study. However, it is noted that the the recycled rubber tyres and the recycled spent ballast used in the lab and field testing were carefully selected, ensuring they are free from contaminants. An array of instrumentation including settlement pegs, horizontal transducers, pressure cells, and accelerometers were installed in both sections [Fig. 15(c)] and connected to an automatic data acquisition system. Protected strain gauge rosettes were bonded to selected tyre cells at predetermined locations to measure the mobilised strains upon the passage of trains. In both track sections, a number of flat pressure cells were placed at different depths (sleeper-ballast interface, within the ballast layer, ballast-TCTF interface and below the capping layer) to measure the vertical stress distribution with depth. More details on track construction and instrumentation can be found elsewhere (Indraratna et al. 2024). Quarried fresh ballast (latite basalt) complying with the revised Australian ballast standard (i.e. 60-graded; AS 2758.7-2015) developed through past research and reported by Indraratna et al. (2011) was then placed to a thickness of about 300mm. The ballast layer was compacted by a vibratory roller before the concrete sleeper-steel rail assembly was constructed at the top, and then the track sections finally filled and levelled with crib ballast.

A locomotive of 22-tonne axle load and two fully-loaded ballast wagons were employed to run over the trial track at a relatively low speed @ 15-20 km/h, given the decelerated speed at the maintenance yard. Loading of the field track by the moving train was completed within 6 days with a total of 1003 passes (in both directions), thus imparting over 6,000 loading cycles. This loading was sufficient to allow the track sections to undergo initial compaction to reach a stable state in terms of the track settlement which was recorded continually.

Measured vertical stress

Figure 16 presents a comparison of vertical stresses measured at different depths for the standard track and TCTF sections. During the initial loading stages (N=1-1000 cycles), the vertical stresses at the TCTF's sleeper-ballast interface (142 - 184 kPa) are slightly less than those of the standard section (172 – 238 kPa), while the vertical stresses at the ballast-capping interface of TCTF (73-137 kPa) are higher than those of the standard section (62-98 kPa). This can be attributed to the significant compression of infilled aggregates within the tyre cells compared to a highly compacted traditional capping material. The initial train passes would allow the infilled aggregates to re-arrange and re-compact within the tyre cell before its hoop stress could be activated. So, in the subsequent loading cycles (N > 1000), the stresses at the sleeper-ballast interface of the TCTF are expected to be higher than those in the standard section. For instance, at N=3000 cycles, the maximum stresses measured in the TCTF section was about 305 kPa, while the standard track experienced a maximum stress that was considerably less (194 kPa) for the same number of loading cycles. In other words, at larger number of loading cycles, the compacted infill (recycled ballast) within the confinement of activated tyre cells (hoop stress measured in the range of 35-40 kPa) had contributed to an increase in stiffness of the TCTF assembly, thereby sustaining a greater vertical stress.

The ability to carry a significantly greater vertical stress by the TCTF compared to a standard capping layer is a tangible long-term benefit. The resulting stress propagated to the underlying saturated soft subgrade would now be diminished, thereby minimising the adverse potential for unacceptable deformation and alleviating the potential for soft soil fluidization (mud pumping) under prolonged cyclic loading (Indraratna et al. 2020). The lateral (radial) stress as measured by pressure cells sandwiched at the interface of 2 tyre cells approached 2 kPa, while that for the standard track was in the proximity of 1.2 kPa. This observation further verified the increased lateral confinement offered by the TCTF. As shown in the bottom part of Fig.16, towards the end of the loading stage (N=6000), an increase in vertical stress (298 kPa) is observed at the sleeper-ballast and ballast-tyre interfaces of the TCTF, in comparison with the standard section (184 kPa). So as expected, the maximum vertical stress (< 50 kPa) transferred to the underlying subgrade soil layer is about 10% smaller in the TCTF track compared to that for the standard section (> 56 kPa). This result further verifies that over time (N>6000), the TCTF stratum would offer a stiffer sub-ballast capping to accommodate increased vertical stress thus ensuring a reduced vertical stress transmission to the softer subgrade, thereby curtailing soil yielding and increasing the substructure stability.

Measured track settlement

Figure 17 shows the comparison of total track settlements measured for the TCTF and standard track sections. During the initial N=2000 loading cycles, the total track settlement in the TCTF increases to 8.6 mm, as compared to 6.1 mm in the standard section. During initial train loading and associated vibrations, the ballast particles can displace, rotate and break, hence the corresponding void structure and the particle contacts change rapidly as shown by DEM studies (Tutumluer et al. 2013, Chen et al. 2023). As mentioned earlier, until the tyre cells are activated to provide the maximum lateral confinement and enhanced stiffenss of the TCTF, the infilled material (i.e. more rounded used ballast) continue to undergo significant compression during initial train loading. However, for the subsequent loading stage (N > 2000 cycles), the settlement tends to stabilise for both sections; the additional settlement at the standard section (2.1 mm) is smaller compared to that of TCTF that still shows some notable settlement (4.1 mm), albeit considerably smaller compared to the initial loading stage (N <1000).

At the end of this loading stage, the total settlement of the TCTF of 12.7 mm is greater than that of the standard track (8.2 mm), but it is emphatically noted that much of the settlement of the former had occurred during the initial loading period. For instance, the settlement of TCTF section for N<1000 is about 6 mm compared to about 3.8 mm of the standard track. Once the infilled aggregates compact tightly against the tyre cell wall (generated hoop stress > 35 kPa for N> 3000), the increased stiffness of the TCTF is significant (28 kPa/mm), compared to that of the conventional capping (21 kPa/mm). These values were measured in the field using pressure cells, strain gauges and settlement pegs, while the stiffnesses are calculated based on the measured stresses and deformation. This further clarifies the longer term efficacy of the TCTF to carry a much higher normal stress (> 300 kPa) compared to standard capping (< 200 kPa). It is noted that in the field trial, the TCTF experienced higher settlement than the standard track (without tyre cells). This is because during initial train loading and associated vibrations, the ballast particles could displace, rotate and break; hence the corresponding void structure and the particle contacts would change rapidly. As mentioned earlier, an increased initial settlement may be due to insufficient compaction of the infill materials inside the tyre cell, causing higher elastic strains initially until the infill aggregates become denser through cyclic loading over time.

Measured track vibration

Figure 18 presents the measured accelerations in the TCTF section as compared to the standard section at the inception of loading (N=1-6 cycles) as well as at the end of loading (N=6000-6006 cycles). The track sections were instrumented with accelerometers on the rail to measure vibrations during the train passage. At the initial loading cycles, significant vibration was recorded for the TCTF (0.046 g) compared to 0.014 g in the standard track [Fig. 18(a)]. This increased vibration in the TCTF corroborates to the increased settlement during the initial loading stage as discussed earlier. However, with increased number of loading cycles, the vibration measured in the TCTF decreased swifty to 0.026 g, while the vibration in the standard track remained relatively unchanged [Fig. 18(b)].

Conclusions

This study had presented the results of large-scale track process simulation tests and field testing with and without the inclusion of tyre cell track foundation (TCTF) infilled with compacted granular mass, i.e., either crushed quarried basalt (Capping 1) or recycled spent ballast (Capping 2), the former being considerably finer in its gradation. On the basis of this study, the following specific conclusions can be drawn:

- The inclusion of TCTF reduced track settlement with both types of infill materials at lower stress levels of up to 25-tonne axle load. At an increased stress level (35-tonne), the Capping-1 infill material showed less settlement compared to Capping-2. TCTF could reduce the lateral displacement from 3.4 mm for conventional capping to 2.3 mm and 2.8 mm for Capping-1 and Capping-2, respectively. This leads to the conclusion that Capping-1 rockfill (crushed basalt) would perform marginally better than Capping-2 (recycled used ballast) in terms of effective settlement control.

- The magnitudes of M_R of the tyre-reinforced specimens (i.e. M_R=275 and 278 MPa for Tests 2 and 3, respectively) were notably higher than that of the unreinforced specimen (M_R=258 MPa). In Stage 4, a slight reduction (3.7 %) in M_R for reinforced specimens was observed when the loading frequency was increased from 10 Hz to 15 Hz but the corresponding M_R values recovered again as the number of loading cycles exceeded N = 80,000 cycles. In contrast, M_R of the unreinforced test specimen dropped noticeably to 214 MPa, and then increased at the subsequent loading cycles (N > 75,000).
- The values of vertical stress transmitted to the top of subgrade showed a reduction of about 34% and 26% for Capping-1 (Test 2) and Capping-2 (Test 3) infilled tyre cell specimens. In real-life practice, this observation translates to the use of TCTF being

particularly advantageous in soft subgrade deposits (e.g. coastal estuarine soils) which may otherwise experience premature yielding in the absence of effective control of the vertical stress distribution with depth.

- The test results showed an increase in damping ratio and energy dissipation properties of the tyre cell stabilised specimens. Tests 2 and 3 with Capping-1 and Capping-2 infill materials resulted in a reduction in ballast breakage index (BBI) by 40.1% and 28.3%, respectively. In practice, this significant reduction in ballast breakage attributed to TCTF implies the benefits of:promoting recycling of waste rubber tyres and cost savings for railway industry.
- Field measurements showed that in comparison to the standard track section, an increase in vertical stress was measured at the sleeper-ballast interface of the TCTF (about 36% compared to the standard track), which helped to reduce the vertical stress transfer to the subgrade soil. Despite the relatively high initial settlement of infilled material within the tyre cells, in the longer term the ability to carry a much larger vertical stress culminates in the tangible benefit of reducing the vertical stress propagation to underlying soft and saturated subgrade, thereby alleviating the potential for excessive deformation.

Data Availability Statement

All of the data, models, and codes that support the findings of this study are available from the corresponding author upon reasonable request. (Test data; field testing results).

Conflicts of Interest

The authors all declare no conflict of interest.

Acknowledgements

The TCTF method was invented by Prof Buddhima Indraratna in collaboration with EcoFlex International (c/o Jim Grant) and is an approved Australian Patent (No. 2018214448). The concept of the track process simulation equipment originally proposed by Prof Indraratna was adopted by CMA Pty Ltd. for its construction and commissioning at the UTS TechLab. This study was conducted under the auspices of the Industrial Transformation Training Centre for Advanced Technologies in Rail Track Infrastructure (ITTC-Rail), c/o Australian Research Council (ARC-IC170100006), and ARC Discovery Project (DP220102862). The early efforts of single tyre testing by Dr Mahdi Biabani and the subsequent computational finite element modelling by Dr Qideng Sun conducted under the supervision of Prof Indraratna at the University of Wollongong are appreciated. The authors acknowledge the close collaboration with Sydney Trains (Transport for NSW) and for their valuable input and help throughout the project. The authors are also thankful to Dr Chathuri and Dr Rakesh for their assistance with the field trial work. The authors are also thankful to the technical staff at the University of Technology Sydney (c/o Dr Mandeep Singh) for their assistance during the experimental program amidst COVID-19 restrictions.

References

Arachchige, C. M. K., B. Indraratna, Y. Qi, J. S. Vinod and C. Rujikiatkamjorn (2022). Deformation and degradation behaviour of Rubber Intermixed Ballast System under cyclic loading. *Engineering Geology*. 307: 106786.

AREA (1974). American Railway Engineering Association: Manual for Recommended Practice. AREMA. Washington, DC.

Arulrajah, A., M. Naeini, A. Mohammadinia, S. Horpibulsuk and M. Leong (2020). Recovered plastic and demolition waste blends as railway capping materials. *Transportation Geotechnics*. 22: 100320.

AS_1726 (2017). Geotechnical site investigations. *Standards Australia*. NSW, Australia.

AS_2758.7 (2015). Aggregates and rock for engineering purposes, Part 7. *Railway Ballast. Standard Australia*. NSW, Australia.

ASTM (2018). Standard Test Method for Determining Performance Strength of Geomembranes by the Wide Strip Tensile Method. ASTM D4885.

ASTM D7928 (2017) Standard test method for particle-size distribution (gradation) of fine-grained soils using the sedimentation (hydrometer) analysis. ASTM D7928, ASTM International, West Conshohocken, PA, USA, DOI: 10.1520/D7928-17.

Bolton, M., Y. Nakata and Y. Cheng (2008). Micro-and macro-mechanical behaviour of DEM crushable materials. *Géotechnique*. 58(6): 471-480.

Brindley, F., E. Mountjoy and G. Mountjoy (2012). COAG Standing Council on Environment and Water Study Into Domestic and International Fate of End-of-life Tyres, Hyder Consulting.

Cai, Y., Xu, L., Liu, W., Shang, Y., Su, N. and Feng, D., 2020. Field Test Study on the dynamic response of the cement-improved expansive soil subgrade of a heavy-haul railway. *Soil Dynamics and Earthquake Engineering*, *128*, p.105878

Chen, J., J. S. Vinod, B. Indraratna, T. Ngo and Y. Liu (2023). DEM study on the dynamic responses of a ballasted track under moving loading. *Computers and Geotechnics*. 153: 105105.

Esmaeili, M., A. Shamohammadi and S. Farsi (2020). Effect of deconstructed tire under sleeper pad on railway ballast degradation under cyclic loading. *Soil Dynamics and Earthquake Engineering*. 136: 106265.

Fontserè, V., A. L. Pita, N. Manzo and A. Ausilio (2016). NEOBALLAST: New High-performance and Long-lasting Ballast for Sustainable Railway Infrastructures. *Transportation Research Procedia*. 14: 1847-1854.

Goryunov, S., Khoreshok, A., Grigoryeva, N., Alitkina, O. (2019). The research of operational temperatures of dump trucks tires. The First Interregional Conference Sustainable Development of Eurasian Mining Regions, DOI: 10.1051/e3sconf/201913401014

Guo, Y., V. Markine, W. Qiang, H. Zhang and G. Jing (2019). Effects of crumb rubber size and percentage on degradation reduction of railway ballast. *Construction and Building Materials*. 212: 210-224.

Henkel, D. and G. Gilbert (1952). The effect measured of the rubber membrane on the triaxial compression strength of clay samples. *Geotechnique*. 3(1): 20-29.

Indraratna, B., and W. Salim. 2003. Deformation and Degradation Mechanics of Recycled Ballast Stabilised with Geosynthetics. Soils and Foundations, 43 (4): 35–46

Indraratna, B., C. M. K. Arachchige, C. Rujikiatkamjorn, A. Heitor and Y. Qi (2024). Utilization of Granular Wastes in Transportation Infrastructure. *Geotechnical Testing Journal*. 47(1): GTJ20220233

Indraratna, B., F. Mehmood, S. Mishra, T. Ngo and C. Rujikiatkamjorn (2022). The role of recycled rubber inclusions on increased confinement in track substructure. *Transportation Geotechnics*. 36: 100829.

Indraratna, B., S. Nimbalkar, D. Christie, C. Rujikiatkamjorn and J. Vinod (2010). Field Assessment of the Performance of a Ballasted Rail Track with and without Geosynthetics. *Journal of Geotechnical and Geoenvironmental Engineering*. 136(7): 907-917.

Indraratna, B., C. Rujikiatkamjorn and T. Ngo (2021). Chullora Technology Precinct -Track Design Innovations. *Sydney Train Report*. 2021.

Indraratna, B., W. Salim, C. Rujikiatkamjorn and (2011). Advanced rail geotechnology–ballasted track, CRC press, Taylor & Francis Group, London, UK.

Indraratna, B., Biabani, M.M. and Nimbalkar, S., (2015). Behavior of geocell-reinforced subballast subjected to cyclic loading in plane-strain condition. *Journal of Geotechnical and Geoenvironmental Engineering*, *141*(1), p.04014081.

Indraratna, B., M. Singh, T. T. Nguyen, S. Leroueil, A. Abeywickrama, R. Kelly and T. Neville (2020). Laboratory study on subgrade fluidization under undrained cyclic triaxial loading. *Canadian Geotechnical Journal*. 57(11): 1767-1779.

Indraratna, B., Q. Sun and J. Grant (2017). Behaviour of subballast reinforced with used tyre and potential application in rail tracks. *Transportation Geotechnics*. 12: 26-36.

Indraratna, B., Q. Sun, A. Heitor and J. Grant (2018). Performance of Rubber Tire-Confined Capping Layer under Cyclic Loading for Railroad Conditions. *Journal of Materials in Civil Engineering*. 30(3): 06017021.

Indraratna, B., C. M. K. Arachchige, C. Rujikiatkamjorn, A. Heitor and Y. Qi (2024). Utilization of Granular Wastes in Transportation Infrastructure. *Geotechnical Testing Journal*. 47(1): GTJ20220233

Jayasuriya, C., B. Indraratna and T. N. Ngo (2019). Experimental study to examine the role of under sleeper pads for improved performance of ballast under cyclic loading. *Transportation Geotechnics*. 19: 61-73.

Jeffs, T. and G. Tew (1991). A review of track design procedures: Sleepers and ballast. *Railways of Australia, Melbourne, Australia*.

Jing, G., L. Qie, V. Markine and W. Jia (2019). Polyurethane reinforced ballasted track: Review, innovation and challenge. *Construction and Building Materials*. 208: 734-748.

Koohmishi, M. and Azarhoosh, A., (2021). Degradation of crumb rubber modified railway ballast under impact loading considering aggregate gradation and rubber size. *Canadian Geotechnical Journal*, *58*(3), p.398-410.

Lackenby, J., B. Indraratna, G. McDowell and D. Christie (2007). Effect of confining pressure on ballast degradation and deformation under cyclic triaxial loading. *Géotechnique*. 57(6): 527-536.

Le Pen, L., G. Watson, A. Hudson and W. Powrie (2018). Behaviour of under sleeper pads at switches and crossings–Field measurements. *Proceedings of the Institution of Mechanical Engineers, Part F: Journal of rail and rapid transit*. 232(4): 1049-1063.

Luo, Z., C. Zhao, W. Cai, Q. Gu, W. Lin, X. Bian and Y. Chen (2023). Full-scale model tests on ballasted tracks with/without geogrid stabilisation under high-speed train loads. *Géotechnique*. 0(0): 1-15.

Maciej, S. (2017). Environmentally friendly polymer-rubber composites obtained from waste tyres: A review. *Journal of cleaner production*. v. 147: pp. 560-571-2017 v.2147.

Moubeké, C. A., A. Nguessong-Nkenfack, G. E. Ntamack, T. Beda and S. Charif D'Ouazzane (2021). Influence of Under Sleepers Rubber Mat on Propagation of Vibrations from a Railway Track Lying on a Semi-Infinite Soft Ground. *Indian Geotechnical Journal*.

Mountjoy, E. (2012). COAG Standing Council on Environment and Water Study into domestic and international fate of end-of-life tyres Final Report. *Energy*. 4: 10.12.

Navaratnarajah, S. K., B. Indraratna and N. T. Ngo (2018). Influence of under sleeper pads on ballast behavior under cyclic loading: experimental and numerical studies. *Journal of Geotechnical and Geoenvironmental Engineering*. 144(9): 04018068.

Ngamkhanong, C. and S. Kaewunruen (2020). Effects of under sleeper pads on dynamic responses of railway prestressed concrete sleepers subjected to high intensity impact loads. *Engineering Structures*. 214: 110604.

Ngo, T., B. Indraratna, M. Coop and Y. Qi (2024). Behaviour of ballast stabilised with recycled rubber mat under impact loading. *Géotechnique*. 0(0): 1-21.

Powrie, W., L. Le Pen, D. Milne and D. Thompson (2019). Train loading effects in railway geotechnical engineering: Ground response, analysis, measurement and interpretation. *Transportation Geotechnics*. 21: 100261.

Powrie, W., L. A. Yang and C. R. I. Clayton (2007). Stress changes in the ground below ballasted railway track during train passage. *Proceedings of the Institution of Mechanical Engineers: Part F: Journal of Rail and Rapid Transit*. 221(2): 247-261.

Presti, D. L. (2013). Recycled tyre rubber modified bitumens for road asphalt mixtures: A literature review. *Construction and Building Materials*. 49: 863-881.

Qi, Y. and B. Indraratna (2023). The effect of adding rubber crumbs on the cyclic permanent deformation of waste mixtures containing coal wash and steel furnace slag. *Géotechnique*. 71(11): 951-960.

Qi, Y., Indraratna, B., Ngo, T., Arachchige, C.M. and Hettiyahandi, S., 2024. Sustainable solutions for railway using recycled rubber. *Transportation Geotechnics*, p.101256.

Qiang, W., G. Jing, D. P. Connolly and P. Aela (2023). The use of recycled rubber in ballasted railway tracks: A review. *Journal of Cleaner Production*. 420: 138339.

Raymond, G. P. (1977). Stresses and deformations in railway track.

Riyajan, S. A., I. Intharit and P. Tangboriboonrat (2012). Physical properties of polymer composite: Natural rubber glove waste/polystyrene foam waste/cellulose. *Ind Crops Prod*. 36(1): 376-382.

Rose, J., B. Su and F. Twehues (2004). Comparisons of railroad track and substructure computer model predictive stress values and in-situ stress measurements. Proceedings of the AREMA 2004 Annual Conference & Exposition, Nashville, TN, September.

Selig, E. T. and J. M. Waters (1994). Track geotechnology and substructure management, Thomas Telford.

Sheng, X.W., Zheng, W.Q., Zhu, Z.H., Luo, T.J. and Zheng, Y.H., (2020). Properties of rubber under-ballast mat used as ballastless track isolation layer in high-speed railway. *Construction and Building Materials*, *240*, p.117822.

Sienkiewicz, M., J. Kucinska-Lipka, H. Janik and A. Balas (2012). Progress in used tyres management in the European Union: A review. *Waste Management*. 32(10): 1742-1751.

Signes, H. C., Fernández, P., Perallón, E. and Franco, R., (2017). Analysis of the vibration alleviation of a new railway sub-ballast layer with waste tyre rubber. *Materials and Structures*, *50*, pp.1-13.

Sol-Sánchez, M., Moreno-Navarro, F. and Rubio-Gámez, M.C., (2015). The use of elastic elements in railway tracks: A state of the art review. *Construction and building materials*, *75*, pp.293-305.

Sol-Sánchez, M., F. Moreno-Navarro, M. C. Rubio-Gámez, N. Manzo and V. Fontseré (2018). Full-scale study of Neoballast section for its application in railway tracks: optimization of track design. *Materials and Structures*. 51(2): 43.

Sol-Sánchez, M., N. H. Thom, F. Moreno-Navarro, M. C. Rubio-Gámez and G. D. Airey (2015). A study into the use of crumb rubber in railway ballast. *Construction and Building Materials*. 75: 19-24.

Sun, Q., B. Indraratna and N. T. Ngo (2019). Effect of increase in load and frequency on the resilience of railway ballast. *Géotechnique*. 69(9): 833-840.

Tutumluer, E., Y. Qian, Y. M. Hashash, J. Ghaboussi and D. D. Davis (2013). Discrete element modelling of ballasted track deformation behaviour. *International Journal of Rail Transportation*. 1(1-2): 57-73.

Wang, T., C. Shi, Y. Yu, G. Xu, S. Liu, H. Wang, J. Yang, M. Gong, Y. Xu and L. Qie (2022). Mechanical properties evaluation of crumb rubber asphalt mixture for elastic trackbed. *Construction and Building Materials*. 331: 127048.

Wong, C. and M. Coop (2020). Development of inter-particle friction in a railway ballast. *Géotechnique Letters*. 10(4): 535-541.

Zhao, C. and Ping, W., (2018). Effect of elastic rubber mats on the reduction of vibration and noise in high-speed elevated railway systems. *Proceedings of the Institution of Mechanical Engineers, Part F: Journal of Rail and Rapid Transit*, *232*(6), p.1837-1851.

List of Tables:

Table 1. Properties of the test materials

Test Materials	d_{max} (mm)	d_{min} (mm)	d_{50} (mm)	C_u	C_c	γ_b (kN/m^3)
Ballast	53	19	45	1.47	1.06	15.6
Capping-1	19	0.075	2.2	15.9	1.42	21.6
Capping-2	53	13.2	40.5	1.59	1.05	16.1
Subgrade	4.75	0.075	0.48	3.87	1.30	17.5

Optimum moisture content: 12%

Table 2. Test Program

Test No.	Tyre cell inclusion	Infill materials	Loading stage	Cumulative number of cycles, N	Axle load (tonne)	Confining pressure (kPa)	Frequency (Hz)
Test 1	No	Capping-1 (crushed basalt aggregate)	1	25000	25	15	10
			2	50000	25	15	15
			3	75000	35	15	10
			4	100000	35	15	15
Test 2	Yes	Capping-1 (crushed basalt aggregate)	1	25000	25	15	10
			2	50000	25	15	15
			3	75000	35	15	10
			4	100000	35	15	15
Test 3	Yes	Capping-2 (recycled spent ballast)	1	25000	25	15	10
			2	50000	25	15	15
			3	75000	35	15	10
			4	100000	35	15	15

Table 3. Particle size distribution (PSD) for ballast before and after the different tests

Sieve Size (mm)	% Passing			
	Initial particle size distribution	Capping-1 (Test 1)	Tyre cell + Capping-1 (Test 2)	Tyre cell + Capping-2 (Test 3)
63	100	100	100	100
53	85	86.7	85.5	85.7
37.5	20	29.2	25.5	26.5
26.5	5	10.3	7.7	8.4
19	0	4.1	3.4	3.9
2.36	0	0	0	0
BBI		0.187	0.112	0.134
Reduction in breakage (%)		-	40.1	28.3

List of Figures

Fig. 11: Variations of dissipated energy (E_d): (a) Stage-1; (b) Stage-2; (c) Stage-3; and (d) Stage-4

Fig. 12: Variations of damping ratio (*D*): (a) Stage-1; (b) Stage-2; (c) Stage-3; and (d) Stage-4

Fig. 13: Vertical stress distributions along the depth in comparison with previous lab and field data

Fig. 14: Particle size distribution curves of ballast sample before and after the tests

Fig. 15. Application of Tyre Cell Track Foundation in Chullora field testing precinct, NSW, Australia: (a) Placement of infilled in the tyre cells laid on geotextile; (b) Typical cross-section of the TCTF; and (c) Instrumentations installed in the TCTF track

Fig. 16. Vertical stress distribution at different granular layer interfaces in TCTF section compared to Standard section

Fig. 17. Total track settlements measured at Chullora test tracks: Standard section vs. TCTF section

Fig. 18. Measured accelerations in the TCTF track compared to the Standard section: (a) at N=1-6 cycles; and (b) at N=6000-6006 cycles

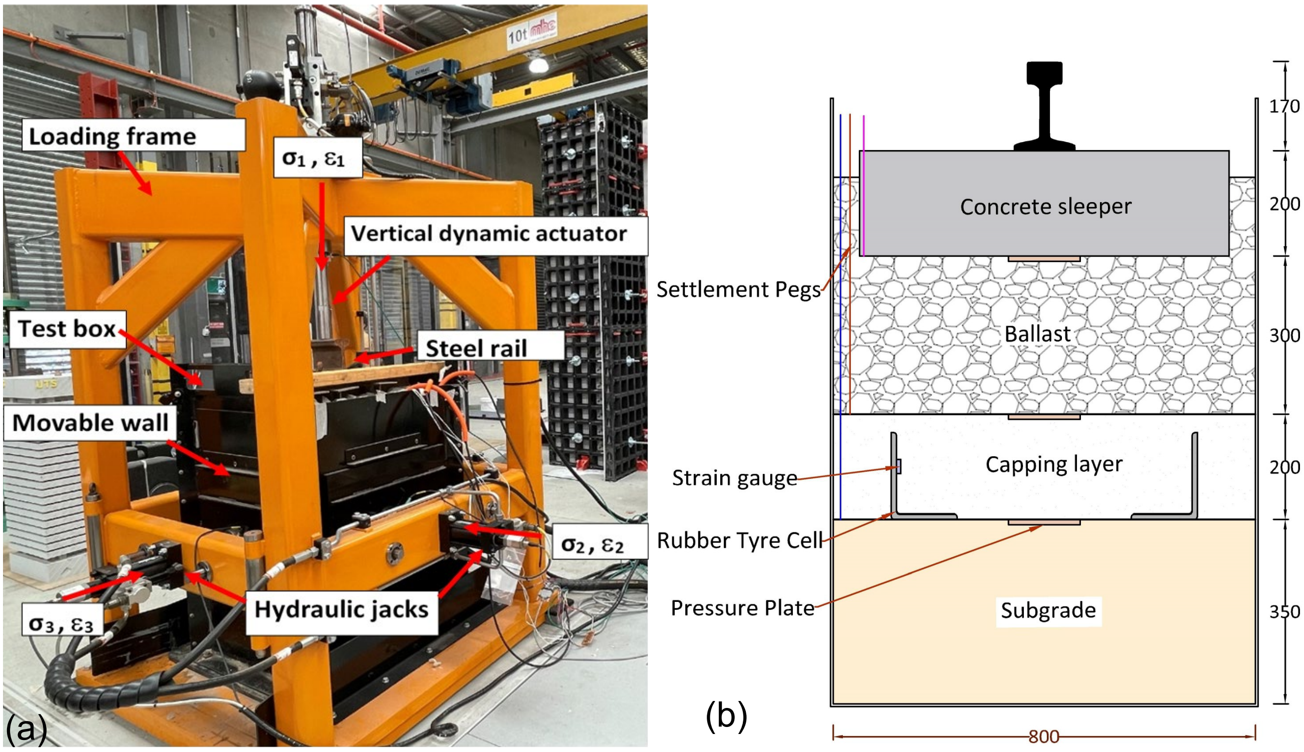

Fig. 1. (a) Large-scale track simulation apparatus; and (b) Schematic diagram of the chamber showing the layer profile (unit: mm)

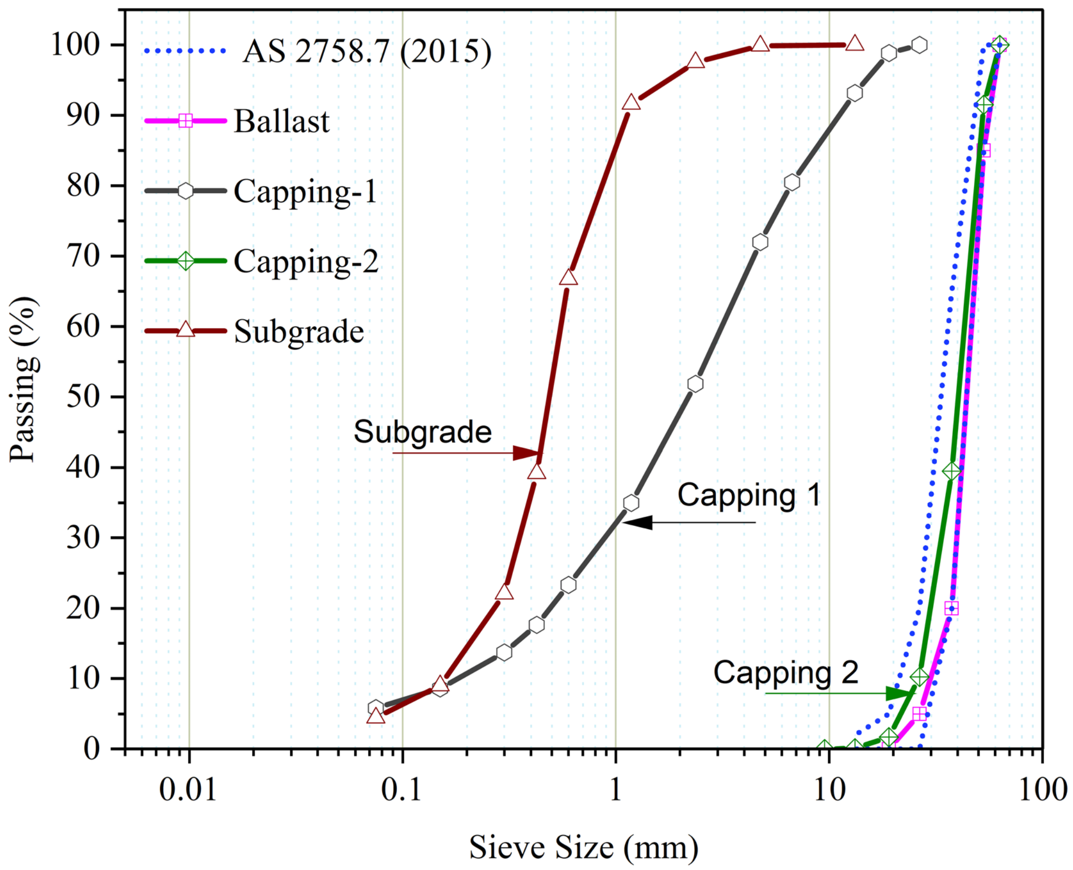

972

973 **Fig. 2.** Particle size distribution curves of ballast, capping materials and subgrade

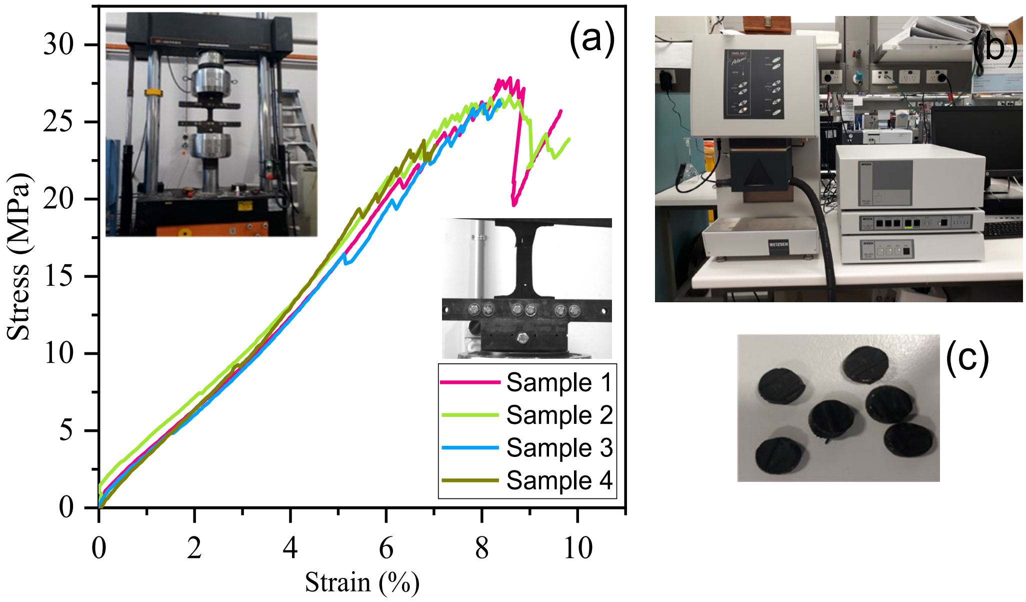

Fig. 3. (a) Tensile stress-strain relationships for the tyre samples; (b) Dynamic Mechanical Analyzer (DMA) to determine damping ratio; and (c) A photo of rubber samples used in DMA testing

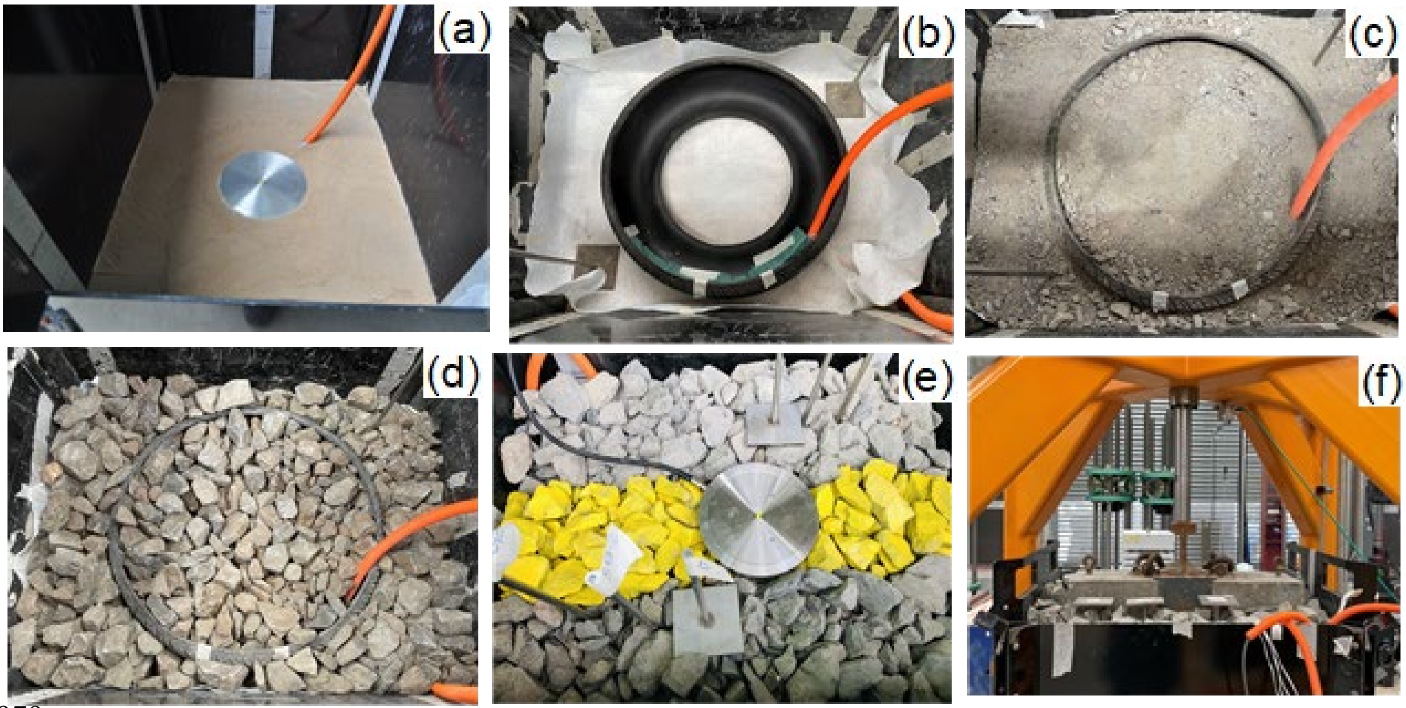

Fig. 4. Sample preparation: (a) Compacted subgrade with pressure cell; (b) Geotextile and strain gauges attached to a tyre cell placed over the subgrade; (c) Capping-1 material inside the tyre cell for Test 2; (d) Capping-2 material inside the tyre cell for Test 3; (e) Pressure plate on ballast layer; and (f) Concrete sleeper with a rail placed within the ballast layer

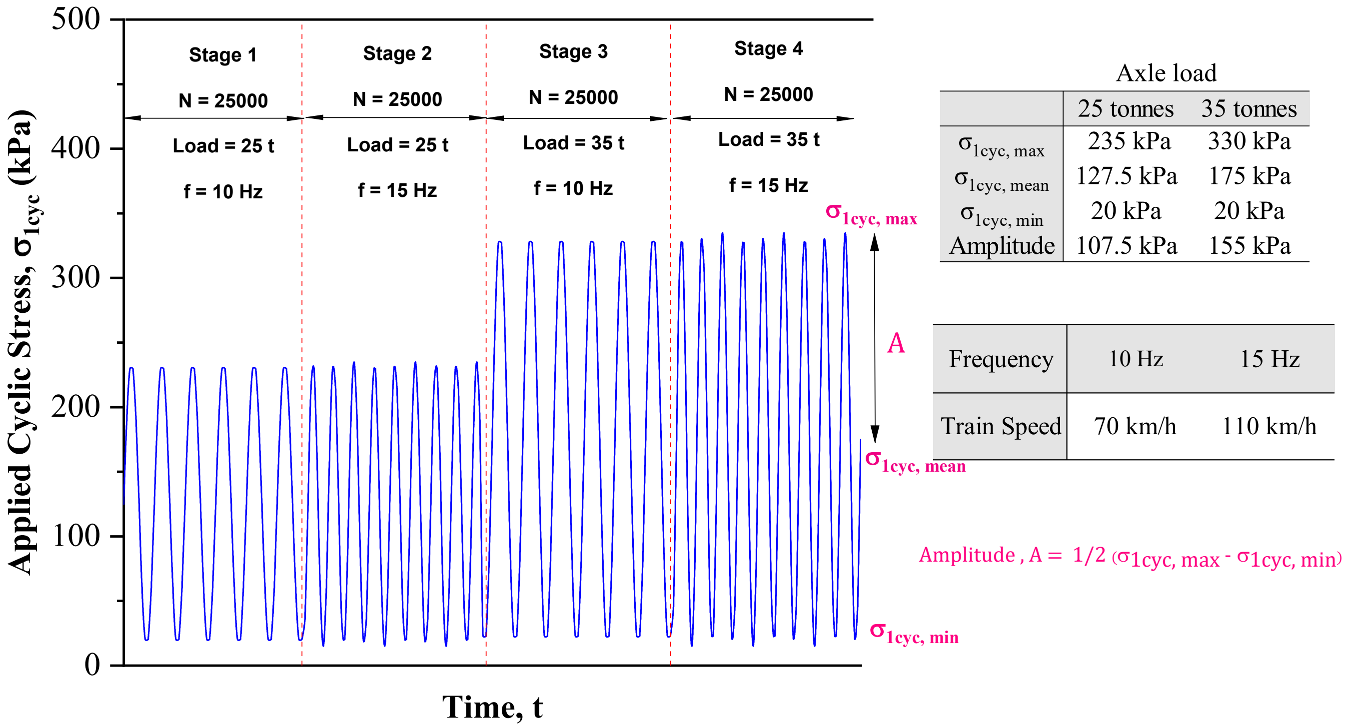

Fig. 5. Multistage cyclic loading program

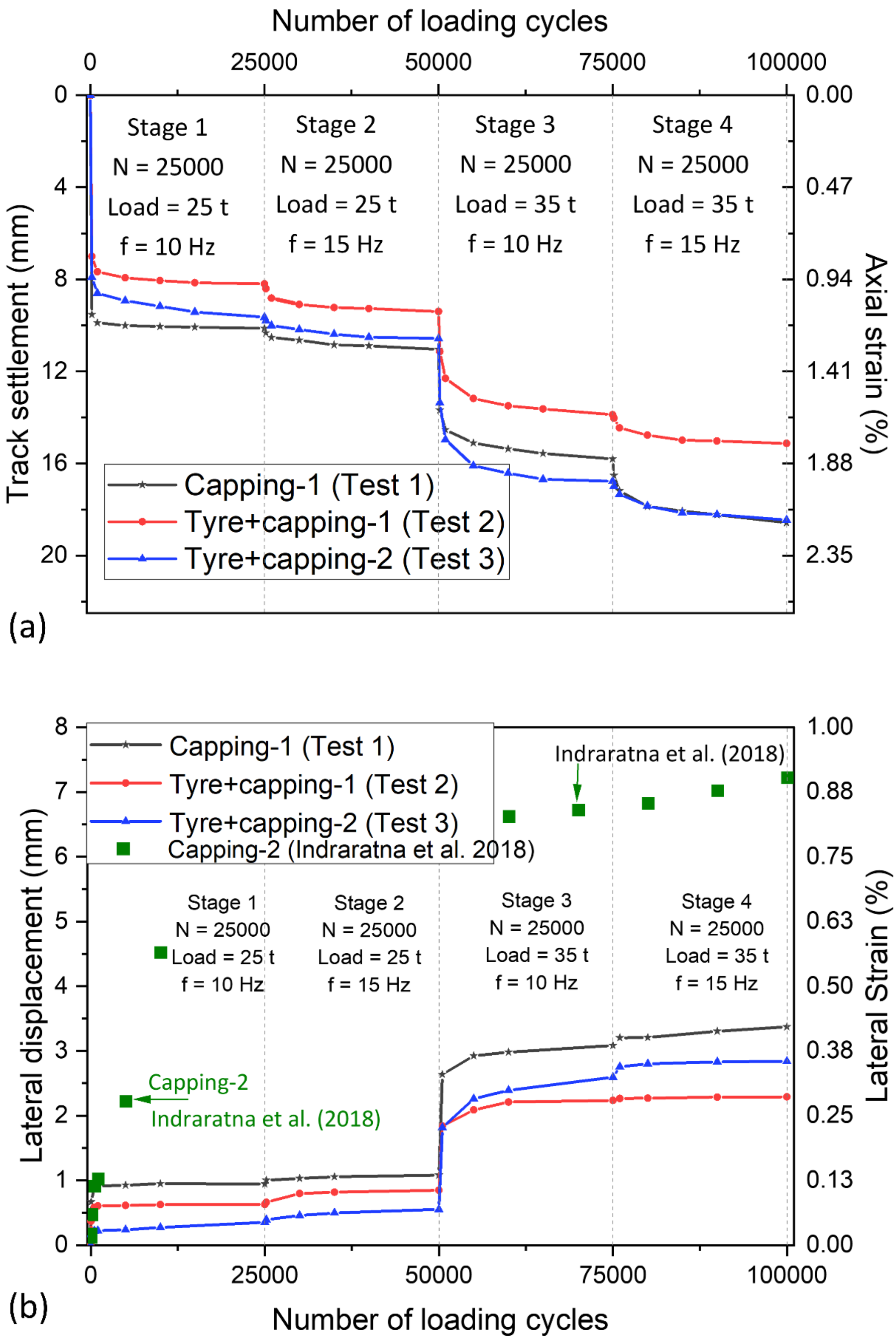

991

992 **Fig. 6.** Measured deformations during the multi-stage loading: (a) track settlements; and (b)

993 lateral displacements

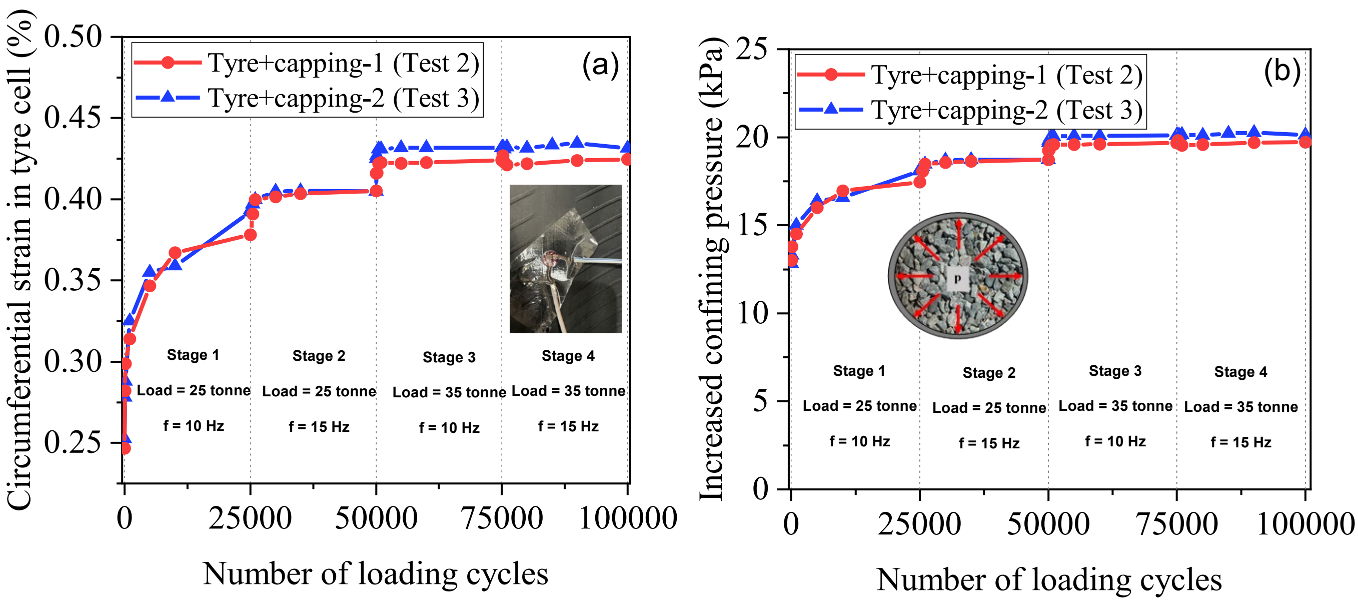

Fig. 7. (a) Mobilised circumferential strain of a tyre cell; (b) variation in increased confining pressure with the number of loading cycles

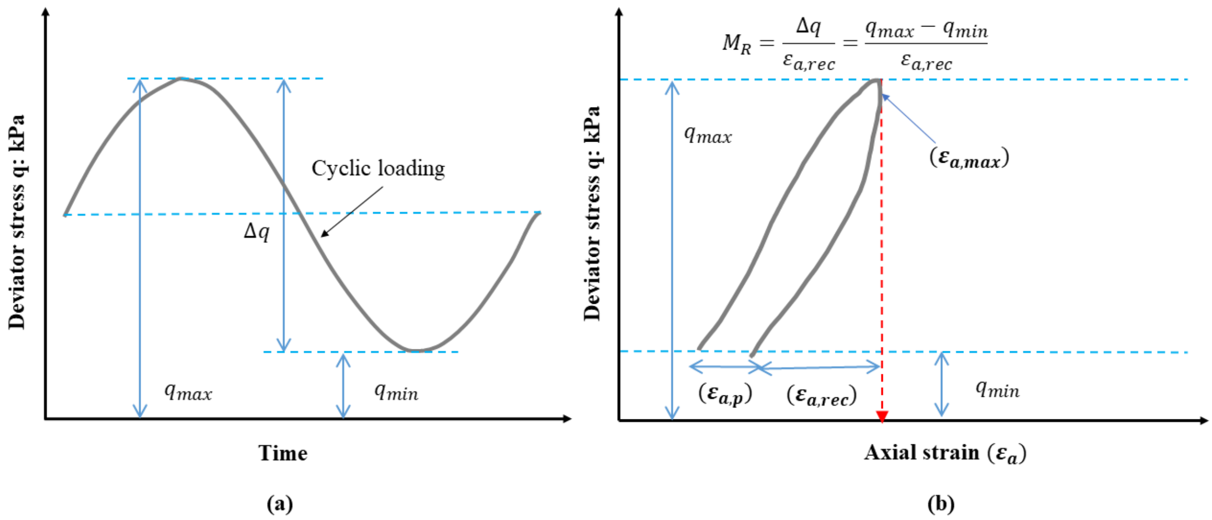

Fig. 8. (a) Applied cyclic loading parameters, (b) calculation of resilient modulus

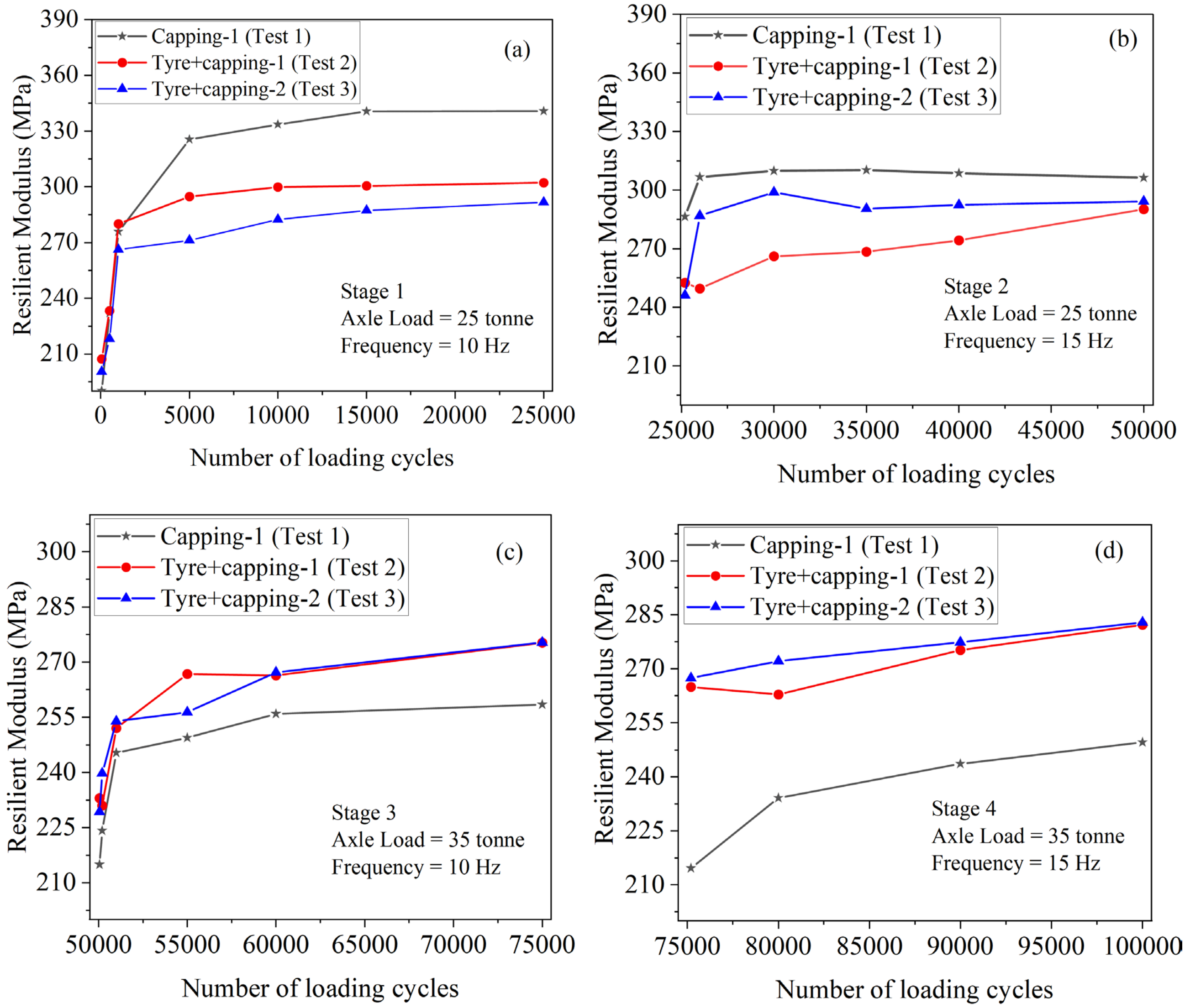

Fig. 9. Measured resilient modulus (M_R) at different loading stages: (a) Stage-1; (b) Stage-2; (c) Stage-3; and (d) Stage-4

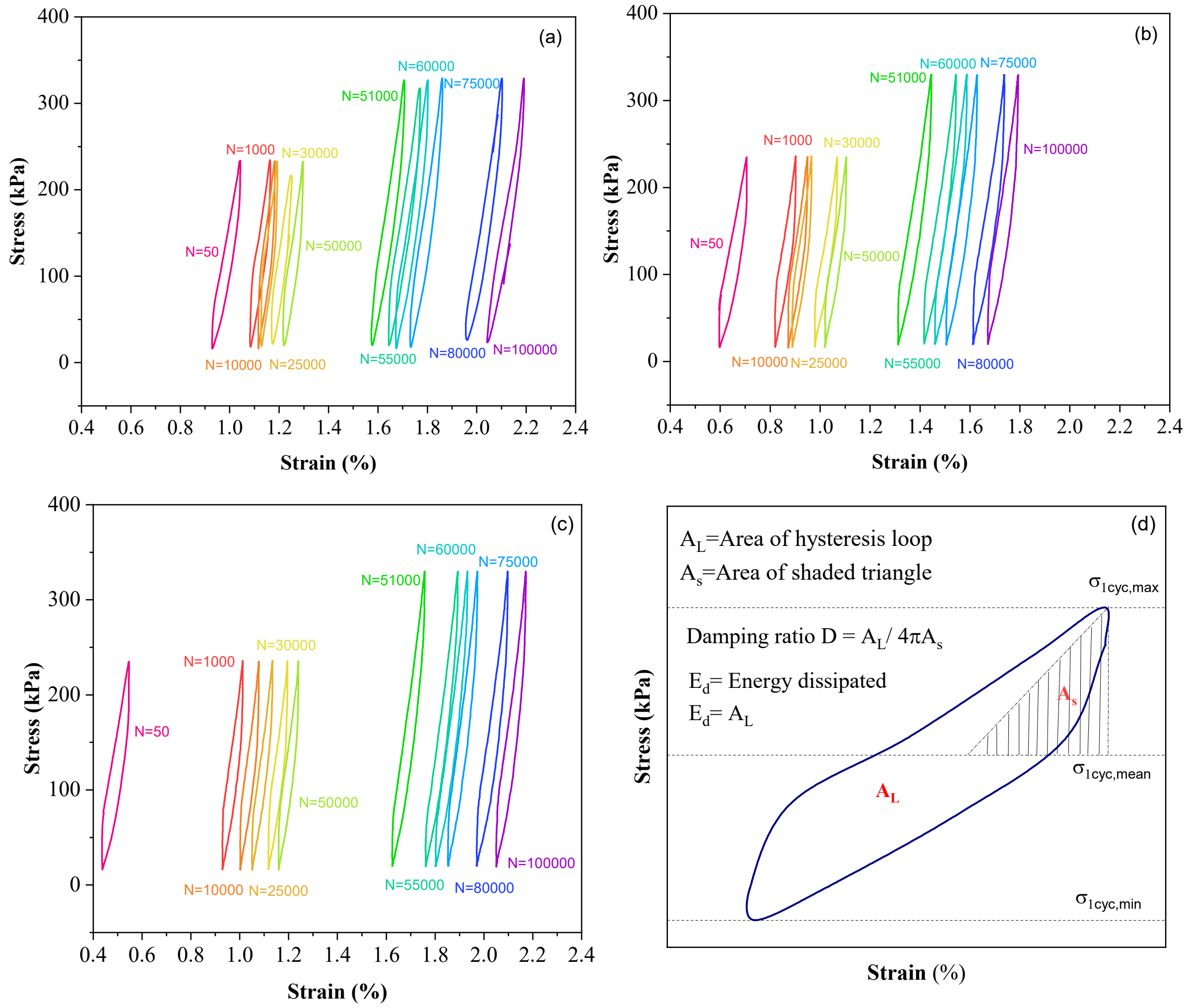

Fig. 10. Hysteresis loops from: (a) Test 1, (b) Test 2, (c) Test 3; (d) schematic diagram of hysteresis loop showing the calculation of damping ratio and dissipated energy

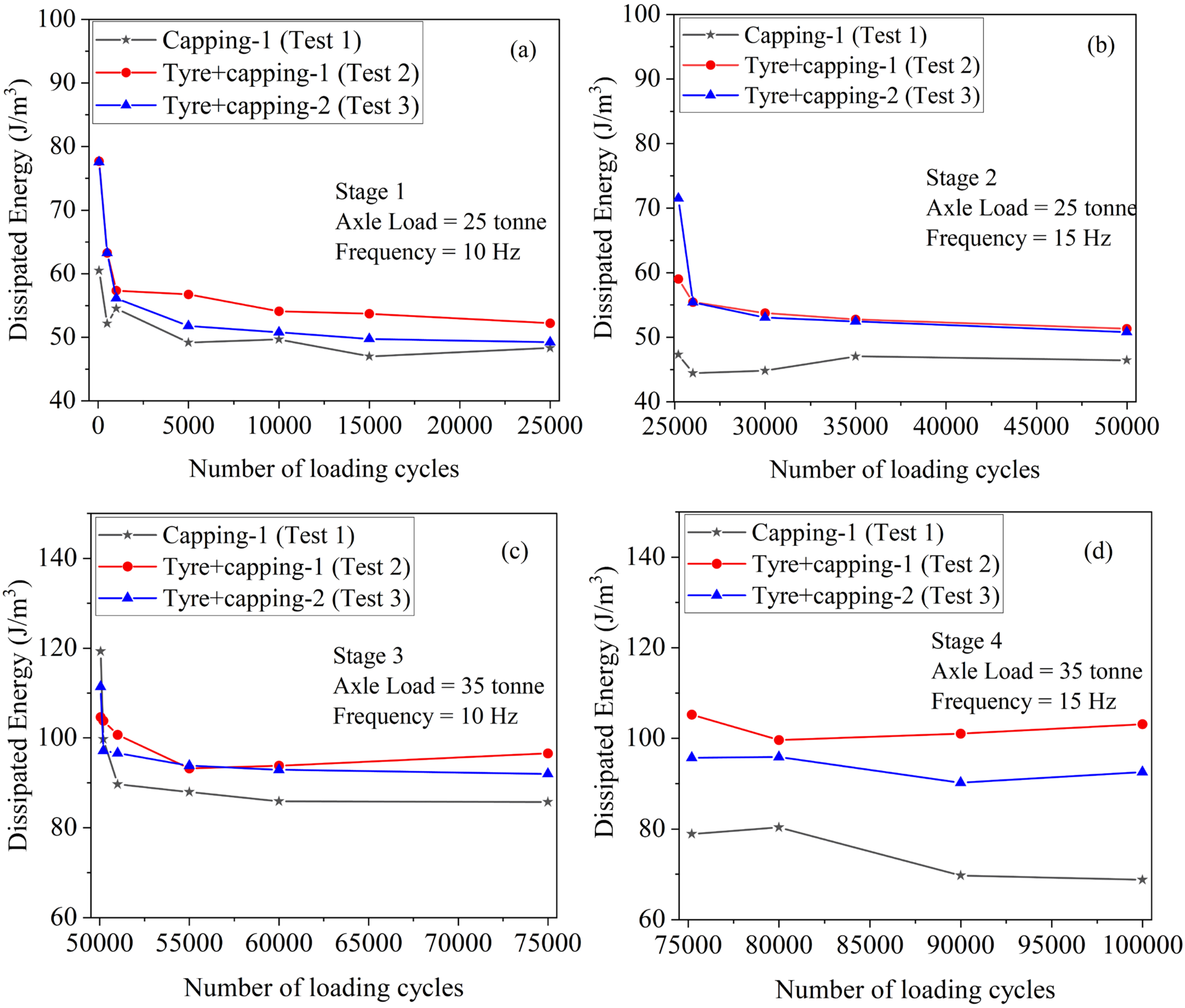

Fig. 11. Variations of dissipated energy (E_d): (a) Stage-1; (b) Stage-2; (c) Stage-3; and (d) Stage-4

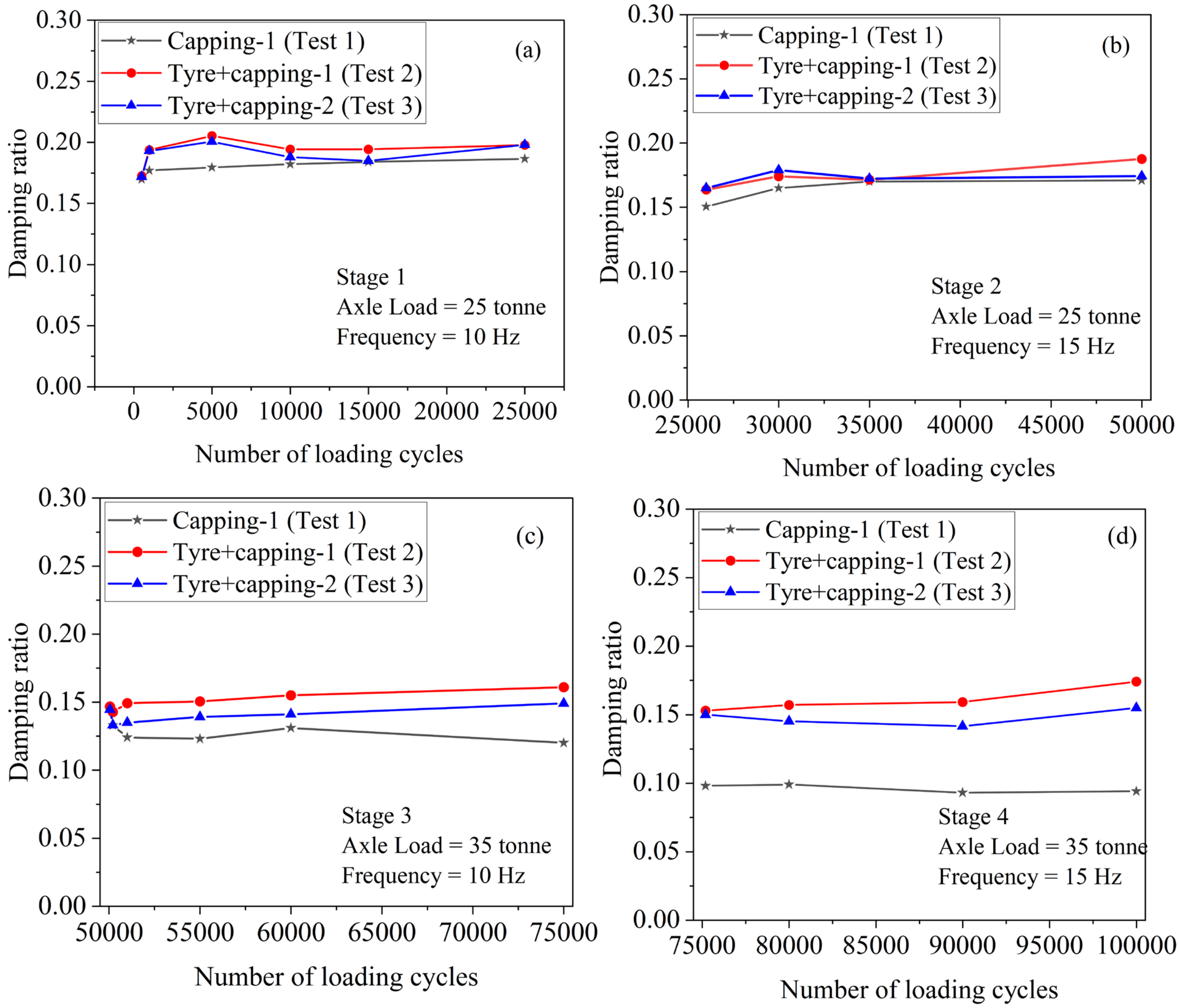

Fig. 12. Variations of damping ratio (*D*): (a) Stage-1; (b) Stage-2; (c) Stage-3; and (d) Stage-4

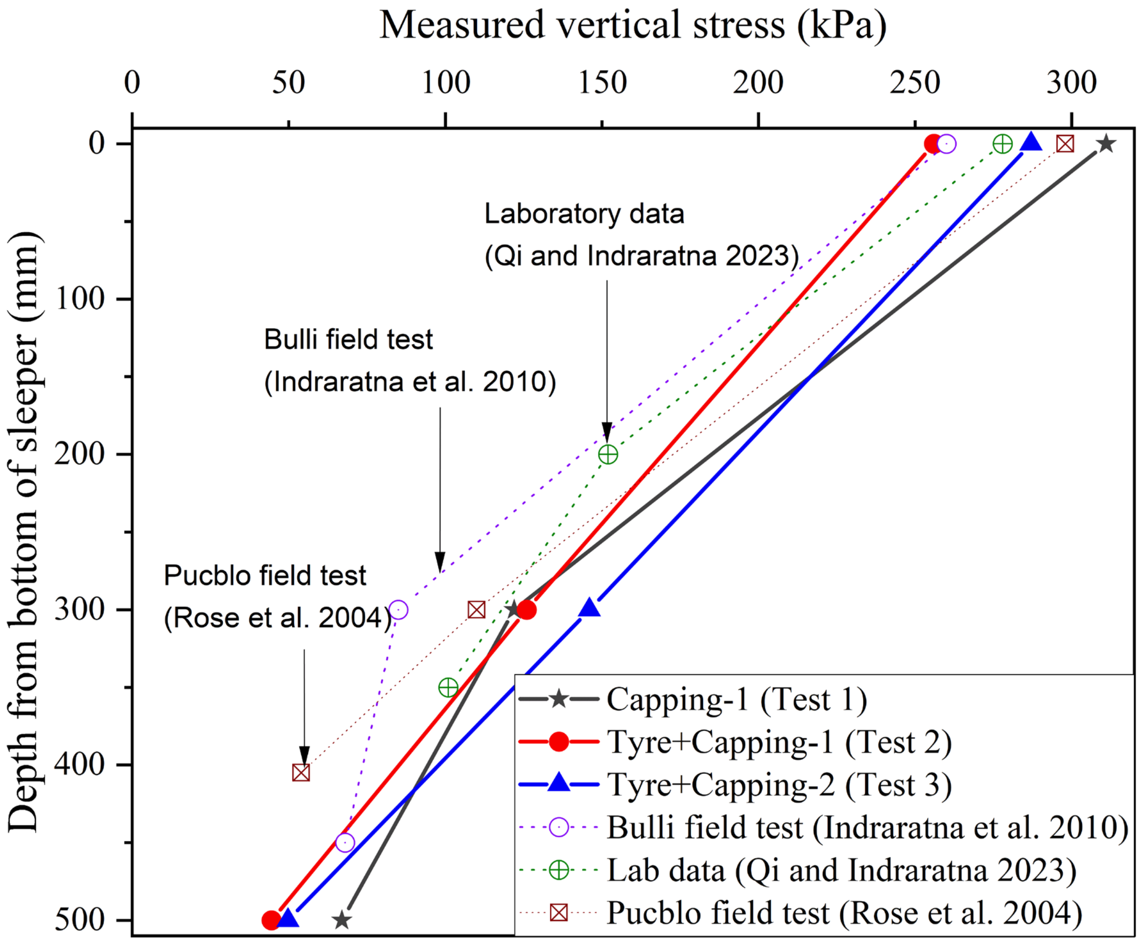

Fig. 13. Vertical stress distributions along the depth in comparison with previous lab and field data

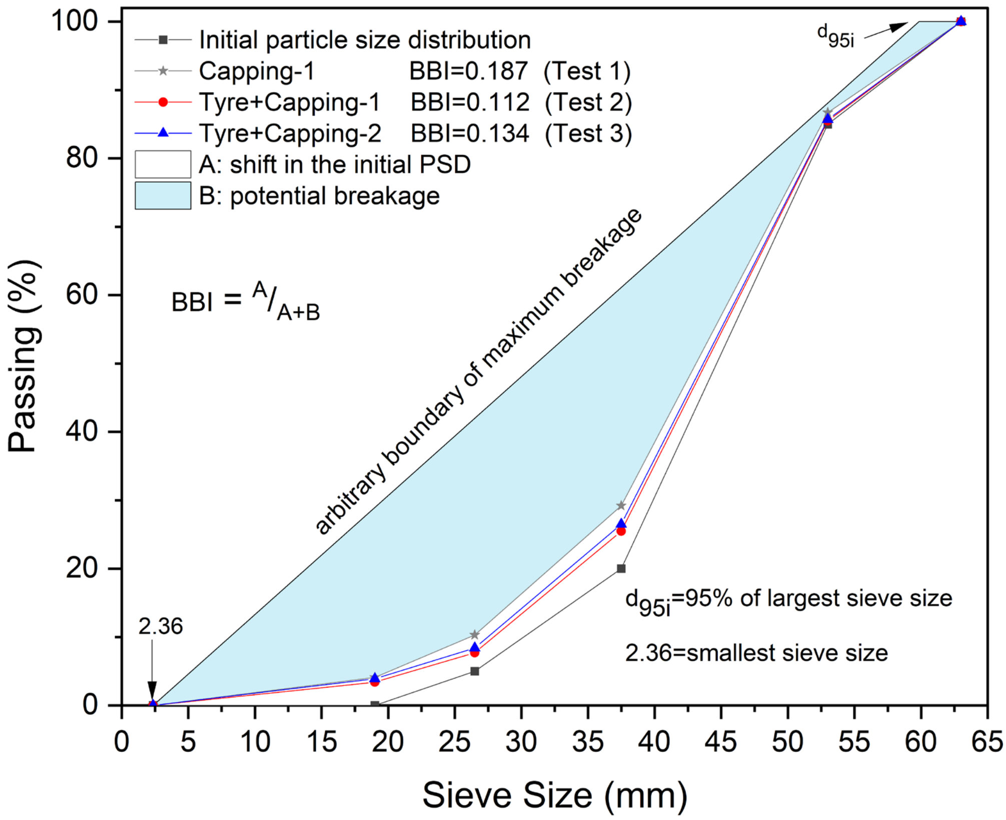

Fig. 14. Particle size distribution curves of ballast sample before and after the tests

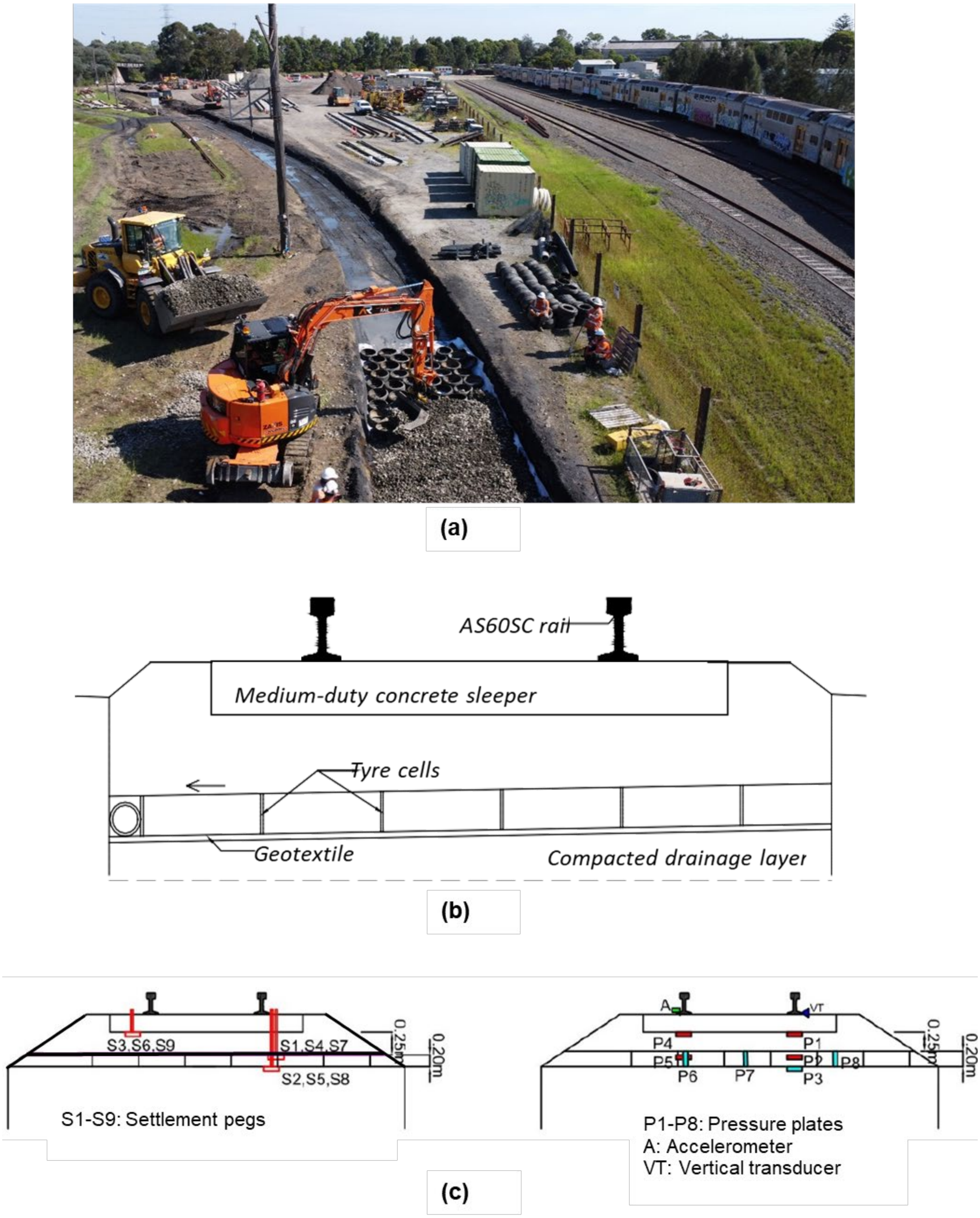

Fig. 15. Application of Tyre Cell Track Foundation in Chullora field testing precinct, NSW, Australia: (a) Placement of infilled in the tyre cells laid on geotextile; (b) Typical cross-section of the TCTF; and (c) Instrumentations installed in the TCTF track

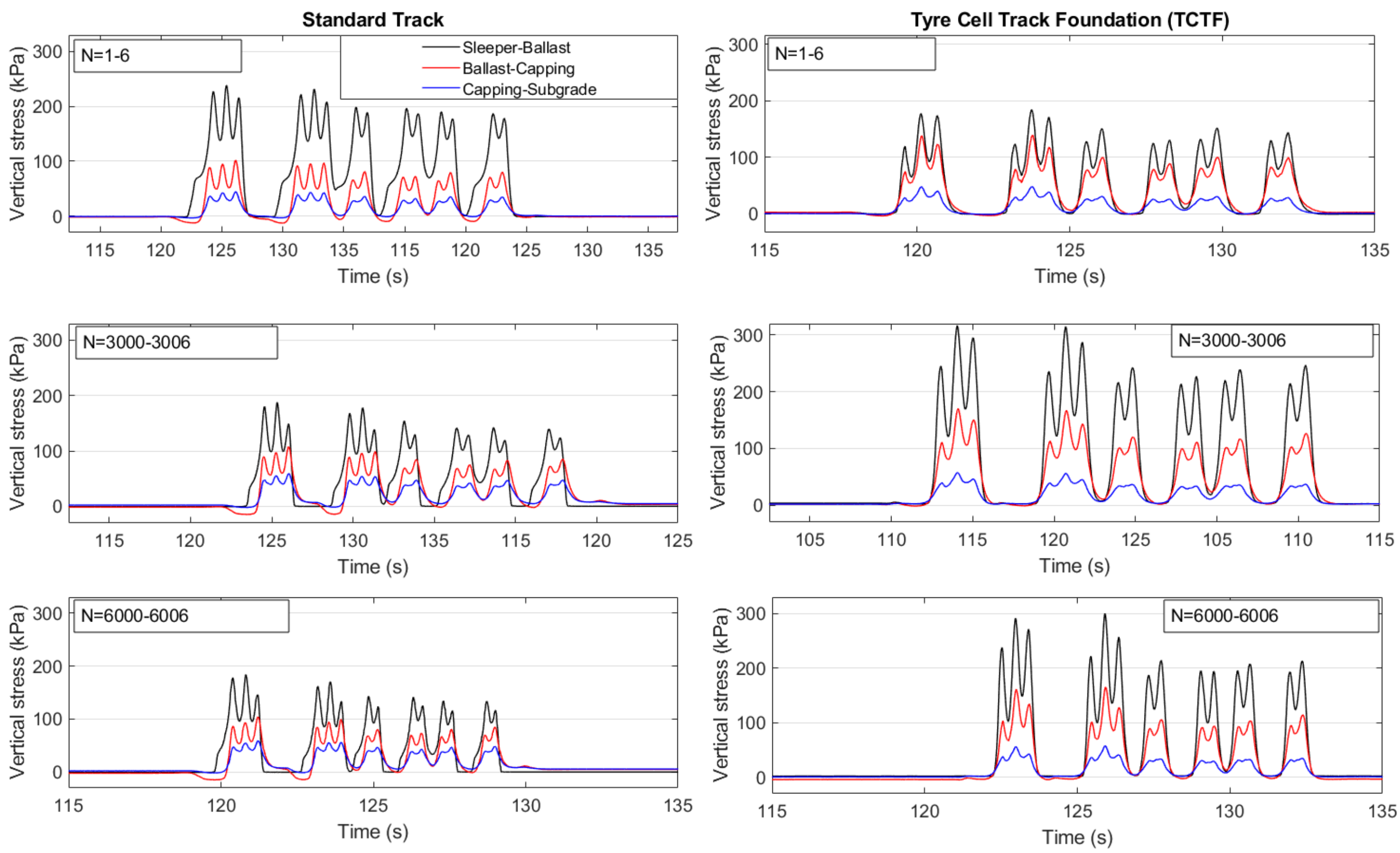

Fig. 16. Vertical stress distribution at different granular layer interfaces in TCTF section compared to Standard section

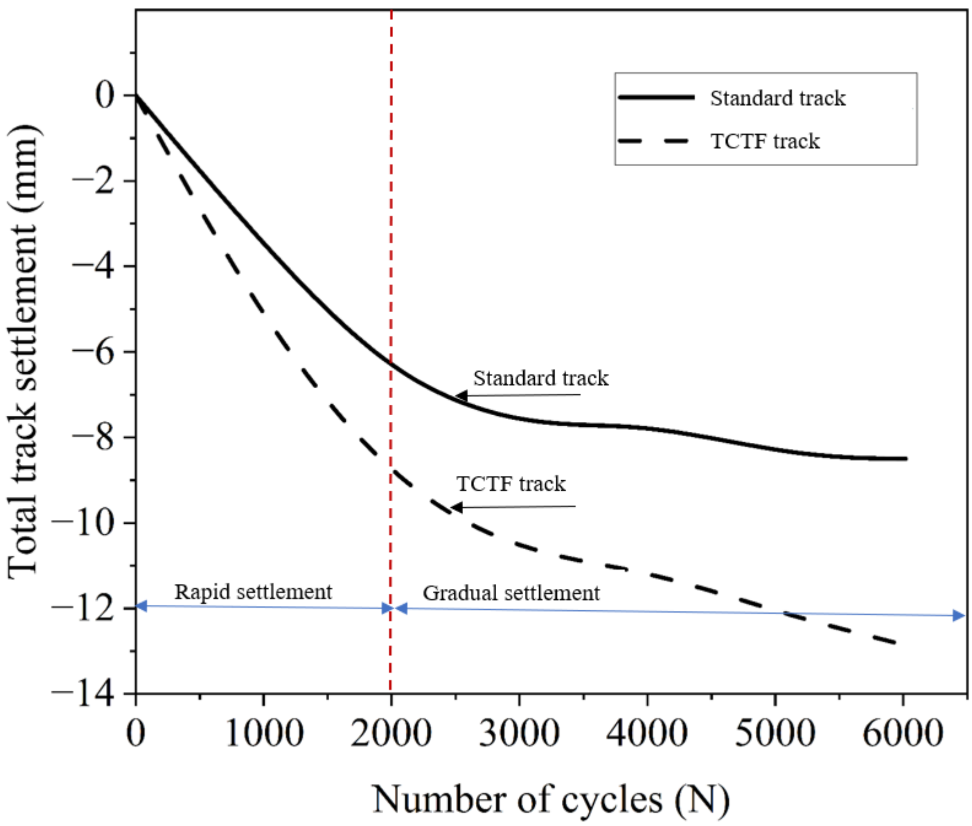

Fig. 17. Total track settlements measured at Chullora test tracks: Standard section vs. TCTF section

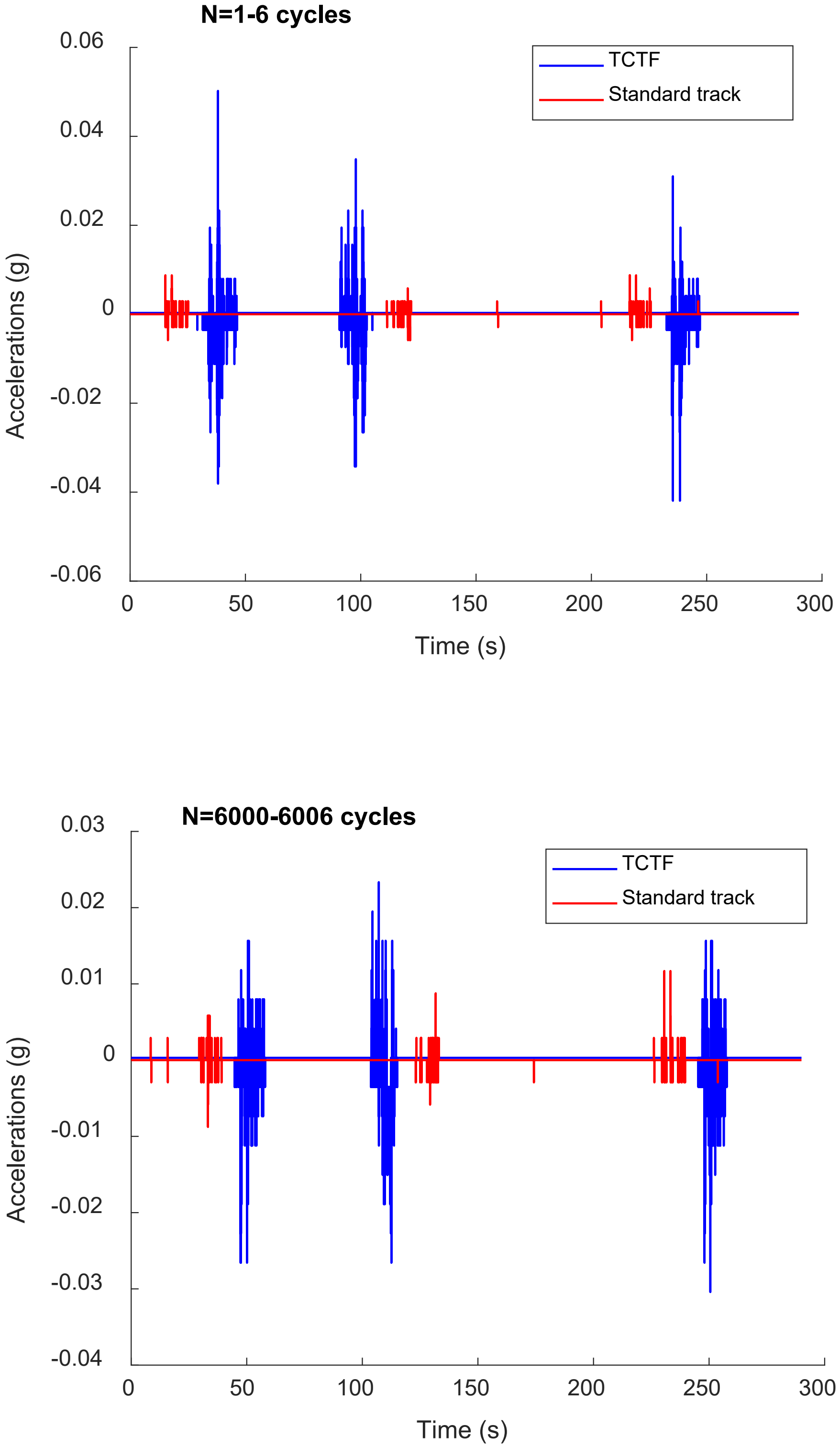

Fig. 18. Measured accelerations in the TCTF track compared to the Standard section: (a) at N=1-6 cycles; and (b) at N=6000-6006 cycles